Atmospheric
Chemistry
and Physics

Open Access

EGU

Detection of water vapour absorption around 363 nm in measured atmospheric absorption spectra and its effect on DOAS evaluations

Johannes Lampel[1,a], Denis Pöhler[2], Oleg L. Polyansky[3,4], Aleksandra A. Kyuberis[4], Nikolai F. Zobov[4], Jonathan Tennyson[3], Lorenzo Lodi[3], Udo Frieß[2], Yang Wang[1], Steffen Beirle[1], Ulrich Platt[2], and Thomas Wagner[1]

[1]Max Planck Institute for Chemistry, 55128 Mainz, Germany
[2]Institute of Environmental Physics, University of Heidelberg, 69120 Heidelberg, Germany
[3]Department of Physics and Astronomy, University College London, Gower St, London WC1E 6BT, UK
[4]Institute of Applied Physics, Russian Academy of Sciences, Nizhny Novgorod, Russia
[a]now at: Institute of Environmental Physics, University of Heidelberg, 69120 Heidelberg, Germany

Correspondence to: Johannes Lampel (johannes.lampel@iup.uni-heidelberg.de)

Abstract. Water vapour is known to absorb radiation from the microwave region to the blue part of the visible spectrum with decreasing efficiency. Ab initio approaches to model individual absorption lines of the gaseous water molecule predict absorption lines up to its dissociation limit at 243 nm.

We present the first evidence of water vapour absorption near 363 nm from field measurements using data from multi-axis differential optical absorption spectroscopy (MAX-DOAS) and long-path (LP)-DOAS measurements. The identification of the absorptions was based on the recent "POKAZATEL" line list by Polyansky et al. (2017).

For MAX-DOAS measurements, we observed absorption by water vapour in an absorption band around 363 nm with optical depths of up to 2×10^{-3}. The retrieved column densities from 2 months of measurement data and more than 2000 individual observations at different latitudes correlate well with simultaneously measured well-established water vapour absorptions in the blue spectral range from 452 to 499 nm ($R^2 = 0.89$), but the line intensities at around 363 nm are underestimated by a factor of 2.6 ± 0.5 by the ab initio model. At a spectral resolution of 0.5 nm, we derive a maximum cross section value of 2.7×10^{-27} cm^2 molec^{-1} at 362.3 nm. The results were independent of the used literature absorption cross section of the O$_4$ absorption, which overlays this water vapour absorption band.

Also water vapour absorption around 376 nm was identified. Below 360 nm no water vapour absorption above 1.4×10^{-26} cm^2 molec^{-1} was observed.

The newly found absorption can have a significant impact on the spectral retrievals of absorbing trace-gas species in the spectral range around 363 nm. Its effect on the spectral analysis of O$_4$, HONO and OClO is discussed.

1 Introduction

The most important greenhouse gas is water vapour. It plays a key role in the radiative balance of the Earth's atmosphere (e.g. Myhre et al., 2013). Due to the large temperature range covered by observations on Earth but also on exoplanets, and due to the spectral extend of observed water vapour absorption, accurate water vapour line lists covering different temperatures over a wide range of wavelengths are necessary. Since water vapour absorption is present in many wavelength regions, precise knowledge of their properties is also required for assessing greenhouse effects. In addition it is required for spectroscopic detection of other trace gases, since their absorption structures often overlap with water vapour absorption. The number of laboratory measurements of water vapour absorption spectra at different temperatures is limited due to technical reasons: experimental measurements of water vapour absorption are not straightforward, as water vapour cannot be compressed to increase its optical depths in a measurement volume at any temperature. Moreover, the absorption cross section is relatively small in certain wavelength ranges, e.g. in the blue and near-UV spectral ranges
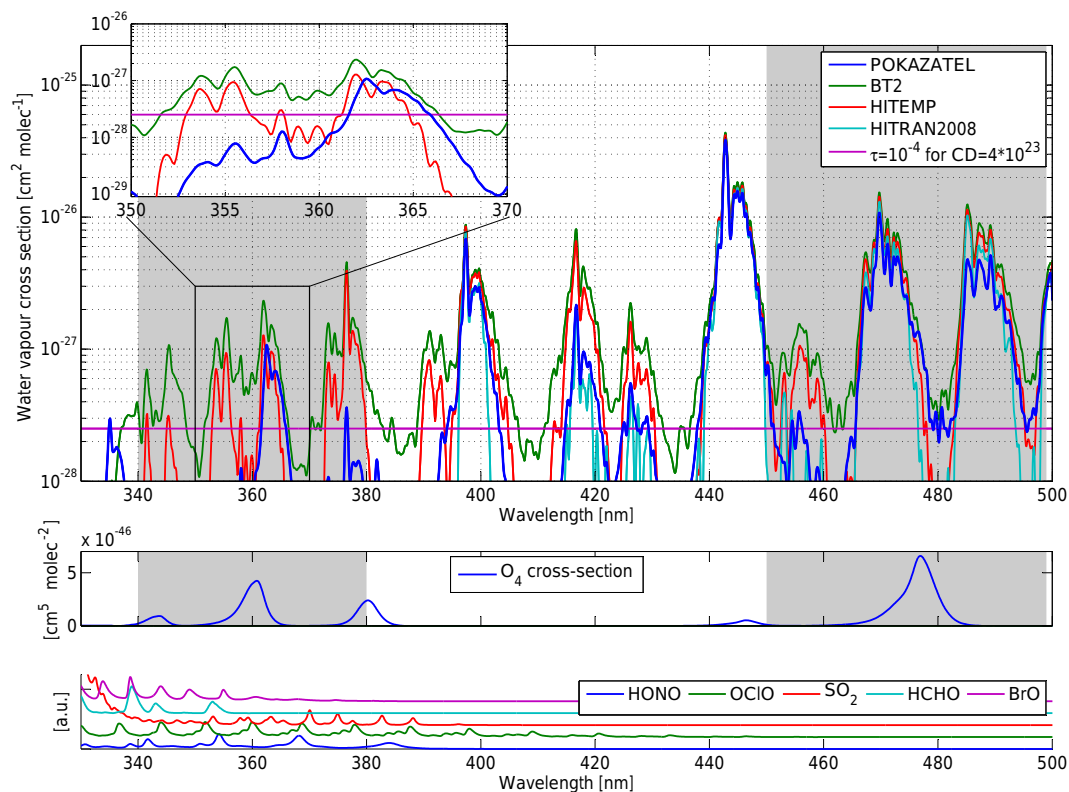
Figure 1. Overview of some recently published water vapour cross sections convoluted to a spectral resolution of 0.5 nm in the spectral interval from 330 to 500 nm. Also indicated is a typical MAX-DOAS detection limit for a differential optical density (OD) of 10^{-4} at a water vapour column density of 4×10^{23} (purple line, top panel). The middle panel shows the O_4 absorption cross section and the lowermost panel shows other absorbers of atmospheric relevance (HONO, OClO, SO_2, HCHO, and BrO) in this spectral range.

that concern us here. The gap between observed absorptions and the available literature absorption cross sections from laboratory measurements can be addressed by means of ab initio models for water vapour absorption lines, which can provide energy (i.e. wavelength), intensity and additional parameters for each absorption line. This is done, e.g., in the HITRAN database (Rothman et al., 2013), where information from measured absorption lines is merged with information from other sources such as ab initio models. In addition to HITRAN, other line-list compilations are also available, such as the GEISA database (Jacquinet-Husson et al., 2008), which lists water vapour absorption lines up to $25\,232\,cm^{-1}$ (down to 396.3 nm).

Lampel et al. (2015b) found systematic structures in the fit residuals in this spectral range below 370 nm with magnitudes of around 5×10^{-4} in multi-axis differential optical absorption spectroscopy (MAX-DOAS) atmospheric observations, which could point towards a tropospheric absorber with absorption structures in this spectral range. The BT2 (Barber et al., 2006) and HITEMP (Rothman et al., 2010) line lists could explain some of the structures, but show inconsistencies. HITEMP is a synthesis of the 2008 edition of HITRAN Rothman et al. (2009) and BT2 with HITRAN

lines replacing BT2 ones where they were available[1]. Still, these two line lists show significant differences between each other, mostly due to the individual line cut-off employed in the HITEMP database (see also Fig. 1). This cut-off removes weak absorption lines from the line list and was introduced for the HITRAN and HITEMP line lists to reduce the number of individual absorption lines for further processing as described, e.g., in Rothman et al. (2010). It removes a large number of weak individual lines below the line intensity cut-off of $10^{-27}\,cm\,molec^{-1}$ for wavelengths shorter than 1 µm (Rothman et al., 2010).

Polyansky et al. (2017) recently developed a computed line list (which we call "POKAZATEL" here, according to the first letters of the name of each author) containing water vapour lines in the spectral range below 400 nm. It is independent of the other sources and is based on a num-

---

[1]The HITRAN 2008, HITEMP and HITRAN 2012 data used here were downloaded from the HITRAN website (http://www.cfa.harvard.edu/hitran/) with the file name for HITRAN 2008 version 2009 "01 hit09.par", HITEMP "01 hitemp.par" and HITRAN 2012 "01 hit12.par". BT2 downloaded from the exomol project (Tennyson and Yurchenko, 2012) http://www.exomol.com/data/molecules/H2O/1H2-16O/

ber of theoretical improvements compared to BT2. BT2 already listed absorptions in this spectral region prior to the publication of POKAZATEL. The POKAZATEL line list differs significantly from BT2 and thus also HITEMP below 380 nm (see Fig. 1). In general, only a few of these lines below 380 nm have also been reported from laboratory measurements (Dupré et al., 2005; Maksyutenko et al., 2012). For a compilation of spectroscopic data see Tennyson et al. (2013). Previous publications, such as HITRAN 2012 (Rothman et al., 2013), do not list water vapour lines below 388 nm.

Recently, Wilson et al. (2016) deduced upper limits for the water vapour absorption in the near-UV by incoherent broadband cavity enhanced absorption spectroscopy measurements in the laboratory. They estimated the water vapour absorption cross section to be smaller than 5×10^{-26} cm^2 molec^{-1} at a spectral resolution of 0.5 nm between 340 and 420 nm. This is significantly smaller than the water vapour cross section measured by Du et al. (2013) between 290 and 350 nm (see Sect. 4.8).

1.1 The POKAZATEL line list

Following up on previous high-quality-computed water line lists (Partridge and Schwenke, 1997; Barber et al., 2006), the POKAZATEL line list (Polyansky et al., 2017) was calculated for the purpose of producing a complete list of water lines involving transitions between all the bound energy levels of H$_2^{16}$O up to dissociation. Until now the most complete water line list, called BT2 (Barber et al., 2006), only covered energy levels up to 30 000 cm^{-1} (333 nm) and rotational quantum numbers, J, up to 50. POKAZATEL covers the entire bound energies up to dissociation – 41 000 cm^{-1} (244 nm) (Boyarkin et al., 2013) and the highest J considered is 72.

POKAZATEL extends BT2 3-fold. First, higher temperatures can be covered by the line list, as higher energy levels are involved and more hot transitions are calculated. Second, for room temperature the spectral range is expanded in the UV region down to about 244 nm. Third, the predictions of the line positions and intensities by POKAZATEL should be considerably more accurate. In particular, POKAZATEL is based on variational nuclear motion calculations performed with the DVR3D program suite (Tennyson et al., 2004).

In order to calculate the line positions and line intensities of the water lines, two inputs into DVR3D are necessary – a water potential energy surface (PES) for the ground electronic state and a dipole moment surface (DMS). A global water PES, covering geometries up to dissociation, is available only from ab initio calculations (Császár et al., 2010) and is not accurate enough for our purposes. POKAZATEL is therefore based on the semi-empirical PES obtained by the fitting to the experimental data up to 41 000 cm^{-1} (Tennyson et al., 2013). The details of the fit are given by Polyansky et al. (2017). In particular, the rms (root mean square) de-

viation for levels below 25 000 cm^{-1}, calculated by this fitted PES, is about 0.03 cm^{-1}, and the levels from 25 000 to 41 000 cm^{-1} are reproduced to within about 0.1 cm^{-1} on average, using measured data from Maksyutenko et al. (2007).

A very accurate, ab initio, global DMS was computed by Lodi et al. (2011) and was used without modification for the POKAZATEL line-list calculation. This DMS has been used to successfully construct comprehensive line lists for H$_2^{17}$O and H$_2^{18}$O (Lodi and Tennyson, 2012), which were included in their entirety in the most recent, 2012, release of HITRAN. A recent laboratory investigation has verified the accuracy of these line lists in the near-infrared (Regalia et al., 2014). However, as discussed below, the intensities predicted by the various line lists have yet to be validated in the near-UV.

1.2 Impact on DOAS measurements of atmospheric trace gases

The absorption lines listed in the UV range in POKAZATEL, BT2 and HITEMP, which are to our knowledge presently not included in DOAS retrievals, could have an effect on the overall measurement errors of several trace-gas retrievals and could lead to systematic biases in the spectral evaluation of tropospheric absorbers in these spectral regions, such as the oxygen dimer O$_2$–O$_2$ (or for short: O$_4$), nitrous acid (HONO), chlorine dioxide (OClO), sulfur dioxide (SO$_2$), formaldehyde (HCHO) and bromine monoxide (BrO). In Sect. 4.11, we discuss these potential interferences. In Fig. 1, absorption cross sections of these species are shown in the two lowermost panels.

In particular, spectral structures at around 360 nm have been observed in atmospheric DOAS measurements before and were explained by erroneous O$_4$ literature cross sections, e.g. an incorrect spectral calibration of the respectively used cross section data (e.g. Wagner et al., 2002). In any case, it could be possibly explained by an unaccounted tropospheric absorber.

1.3 Outline

Based on our field measurements combined with the POKAZATEL water vapour line list, which yields new information about water vapour absorption below 390 nm, we make an attempt to answer the following questions:

1. Are the water vapour absorption bands near 335, 363 and 376 nm found in atmospheric DOAS measurements?

2. Is the magnitude of these absorptions in agreement with measurements in other wavelength ranges? (cf. Lampel et al., 2015b, for the blue spectral range)

3. How well is the shape and the magnitude of the measured absorption bands reproduced by the line lists?

4. What are the consequences for the spectral retrieval of other trace gases in the same spectral region (as, e.g., O_4, HONO and OClO)?

2   Atmospheric DOAS measurements

The data analysed here were collected during three different field campaigns, where different DOAS instruments were used.

1. MAX-DOAS data from cruises ANT XXVIII/1-2 (Naggar, 2012; Kattner, 2012) of the research vessel *Polarstern*, which covered latitudes from 54° N (northern Germany) to 70° S (coastal Antarctica).

2. MAX-DOAS data from the "Surface Ocean PRocesses in the ANtropocene" (SOPRAN) cruise M91 with the research vessel *Meteor* in the Peruvian upwelling region in December 2012 (Bange, 2013).

3. Long-path (LP)-DOAS measurements were analysed for water vapour using data from a dedicated measurement period in Heidelberg in August and September 2015 (further called *HD15*).

An overview of the instruments used is given in Table 1. Both MAX-DOAS cruises were largely unaffected by anthropogenic pollution, which avoids interferences of high-NO_2 absorption structures in the data evaluation.

Due to the small latitudinal and temporal extent of cruise M91 (cf. Table 1 and Fig. 2), the variation of water vapour volume-mixing ratios (VMRs) was small. The VMR was, according to the meteorological station onboard, between 1.6 and 2.4 %. Therefore, observed differential slant column densities (dSCDs; Sect. 3) of H_2O and O_4 correlate well due to changes in the effective light-path lengths and cannot be unambiguously disentangled. In a first-order approximation, the O_4 dSCD is proportional to the effective light-path length, the H_2O dSCD is proportional to the light-path length as well, but also to the absolute humidity along the light path (Eq. 2). The campaign ANT XXVIII/1-2 took place along a cruise track from Bremerhaven, Germany, to Antarctica. It allows one to distinguish actual water vapour absorption from systematic errors of other trace gases, such as the absorption of O_4. Water vapour VMRs were found between 0.5 and 3.0 % according to the meteorological station onboard. The MAX-DOAS instrument onboard *Polarstern* has a lower spectral resolution of 0.7 nm (UV) and 0.9 nm (VIS). It has the advantage of a wider spectral range allowing for independent simultaneous observations of H_2O and O_4 at around 361 and 477 nm due to the spectral overlap of both absorbers (cf. Fig. 1).

Dedicated LP-DOAS measurements were performed in Heidelberg in August and September 2015. The advantage is the high spectral resolution of 0.2 nm and the well-defined
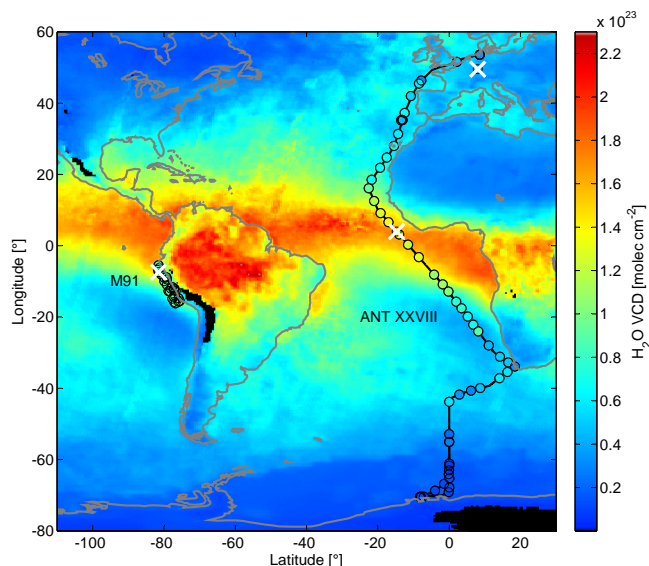

Figure 2. Measurement overview: the cruise track of M91 (Peruvian Upwelling) and ANT XXVIII/1-2 (Atlantic) is shown; additionally, the location of the LP-DOAS measurements in Heidelberg, Germany, is marked (white cross in the north-eastern corner of the map). The background shows GOME-2A H_2O vertical column densities (VCDs) (Wagner et al., 2003) averaged from November to December 2011 (time during ANT XXVIII/1-2). The locations of the measurements shown in Figs. 3 and 5 are also marked by white crosses. Daily error-weighted averages of H_2O / O_4 dSCD ratios (measured in the wavelength range from 340 to 380 nm at 3° telescope elevation, corrected according to Fig. 6) are shown as circles and converted to a VCD assuming an exponential water vapour concentration profile with a scale height of 2 km.

light path of these active measurements. However, high-NO_2 concentrations can cause spectral interferences and the range of absolute water VMRs is relatively limited (see Sect. 4.1).

3   The DOAS Method

The DOAS method (Platt and Stutz, 2008) relies on attenuation of light with a wavelength λ from suitable light sources (intensity I_0) by absorbers within the light path according to Lambert–Beer's law $I(\lambda) = I_0(\lambda) \cdot \exp(-\tau(\lambda))$. The optical density (OD) $\tau(\lambda)$ is calculated from a reference spectrum $I_0(\lambda)$ and a measurement spectrum $I(\lambda)$, $\tau(\lambda) = -\ln \frac{I(\lambda)}{I_0(\lambda)}$. The measured OD of the broadband extinction and scattering by molecules and particles is represented by a broadband polynomial $p(\lambda)$, or the measured OD is filtered into a broadband and a narrow-band contribution. Characteristic absorption features of different absorbing trace-gas species with the total cross section $\sigma_i(\lambda)$ are then used to determine their respective concentrations $c_i(l)$ along the light path L:

$$\tau(\lambda) = \sum_i \sigma_i(\lambda) \int_0^L c_i(l)\mathrm{d}l + p(\lambda). \tag{1}$$

Table 1. Campaigns of which measurements were used. The cruise tracks of the shipborne MAX-DOAS measurements are shown in Fig. 2.

Name	Type	Location, time	Spec. range [nm]	Spec. resolution [nm]	Spectrograph (focal length)	H_2O VMR %
ANT XXVIII/1-2	MAX-DOAS	Atlantic 54–70° S October–December 2011	277–413 390–617	0.7 0.9	OMT $f = 60\,\mathrm{mm}$	0.5–3.0
M91	MAX-DOAS	Peru, coastal upwelling 5° S, 82° W–16° S 75° W 1–25 December 2012	324–467	0.45	Acton 300i $f = 300\,\mathrm{mm}$	1.6–2.4
HD15	LP-DOAS	Heidelberg 49° N, 8° 43′ W August + September 2015	329–371 426–465	0.2 0.2	Acton 300i $f = 300\,\mathrm{mm}$	0.4–1.3

The column density $S_i = \int_0^L c_i(l)\mathrm{d}l$ is calculated by a fitting routine, which is applied to data from a given wavelength interval with a width of several nanometres to several tens of nanometres. The absorption path L is known for LP-DOAS measurements and can be estimated or calculated from radiative transfer models for MAX-DOAS measurements. The high-resolution literature cross sections $\sigma_{L,i}$ are convoluted with the measured instrument function H of the respective set-up to obtain $\sigma_i = H \otimes \sigma_{L,i}$, the absorption cross section as it would be determined by the instrument.

The instrument slit function is usually measured by observing individual atomic emission lines of mercury, which have a spectral width that is 2 orders of magnitude smaller than the resolution of the instrument (Sansonetti et al., 1996).

LP-DOAS measurements (Sect. 3.1) have the advantage of a well-defined light path and the possibility of measurements at night, but typically do not yield the small measurement errors of slant column densities (SCDs) like in MAX-DOAS (Sect. 3.2) observations. The disadvantage of MAX-DOAS measurements is that their effective light-path length depends on various factors, such as atmospheric state (aerosols, clouds), which are often not known precisely. This needs to be explicitly considered in the data evaluation (Sect. 4.2).

The spectral analysis was done using the DOASIS software package (Kraus, 2006).

3.1 LP-DOAS Measurements

The LP-DOAS instrument is based on an artificial light source (here a laser-driven light-source Energetiq LDLS-EQ-99). The light is sent by a telescope through the atmosphere to a retroreflector and reflected back to the same telescope. Thus, the measured atmosphere is in-between the telescope and retroreflector. The received light is transferred to a spectrograph. A measurement sequence consists of four spectra: atmospheric spectrum over the distance to the retroreflector, light-source spectrum, atmospheric background spectrum (i.e. measurements with the light source switched off or blocked) and light-source background spectrum. The correc-

tion of the atmospheric and light-source spectra with background spectra ensures independence from external sunlight, dark current and other instrumental properties (Pöhler et al., 2010).

A description of the LP-DOAS instrument used here can be found in Pöhler et al. (2010) and Eger (2014). The total light path used for the measurements reported was 6.12 km long: above the city of Heidelberg from the roof of the Institute of Environmental Physics to retroreflectors mounted at the train station "Molkenkur" and back to the institute.

The optical density $\tau(\lambda)$ is calculated from a background-corrected light-source spectrum and a background-corrected atmospheric spectrum and filtered by a binomial high pass with 1000 iterations. The convoluted and high-pass-filtered literature cross sections listed in Table 2 are then fitted in the respective fitting interval to the corrected OD.

3.2 MAX-DOAS Measurements

Hönninger and Platt (2002) described the method of MAX-DOAS measurements, which improve the sensitivity of passive DOAS observations at altitude ranges close to the instrument (i.e. up to a few kilometres). It uses scattered sunlight collected by a telescope pointing towards the sky at different elevation angles α. The horizon is here defined as $\alpha = 0°$ and the zenith viewing direction as $\alpha = 90°$. Each elevation has a different sensitivity for absorptions in different heights of the atmosphere. Low-elevation angles have a higher sensitivity to absorbers close to the surface because the additional light path compared to a zenith spectrum recorded at the same time and location is mostly located within the lowermost layers of the atmosphere (Hönninger et al., 2004).

The SCD is defined as the integral over the concentration c_i along the light path L and is hence given in units of molecules cm^{-2}.

$$S = \int_L c_i(s)\mathrm{d}s \tag{2}$$

Table 2. Retrieval wavelength intervals and reference spectra for the MAX-DOAS and LP-DOAS measurements. Literature cross sections listed in brackets were used for sensitivity studies.

	T [K]	MAX-DOAS O_4 / H_2O	MAX-DOAS O_4 / H_2O	MAX-DOAS HONO	MAX-DOAS BrO	MAX-DOAS OClO	LP-DOAS H_2O	LP-DOAS H_2O	
Wavelength interval [nm] Start	Start	340	452	337	332	332	356	441	
	End	380	499	375	358	370	370	450	
H_2O vapour	298		×					×	HITEMP (Rothman et al., 2010)
		×		×	×	×	×		Polyansky et al. (2017)
O_4	293	×	×	×	×	×	×	×	Thalman and Volkamer (2013)
	273	(×)					(×)		
	203	(×)							
	287	(×)							Hermans et al. (2003)
	296	(×)							Greenblatt et al. (1990)
$O3$	223	×	×	×	×	×			Serdyuchenko et al. (2014)
	243			×	×	×			
	293						×		
HCHO		×		×	×	×	×		Chance and Orphal (2011)
HONO				×		×			Stutz et al. (1999)
BrO		×		×	×	×			Fleischmann (2004)
OClO						×			Bogumil et al. (2003)
SO_2				(×)					Vandaele et al. (2009)
NO_2	293	×	×	×	×	×	(×)		Vandaele et al. (1998)
NO_2	293						×	×	Voigt et al. (2001)
NO_2 absorption cell	293						(×)		
Ring spectrum at	273	×	×	×	×	×			DOASIS (Kraus, 2006)
	243	×		×	×	×			which uses Bussemer (1993)
Ring spectrum $\cdot \lambda^4$		×	×	×	×				Wagner et al. (2009)
Polynomial degree		3	3	5	3	4	3	3	
Add. polynomial degree		1	1	1	1	1	0	0	

From MAX-DOAS measurements dSCDs can be calculated for each fitted trace gas: a Fraunhofer reference spectrum (we follow the customary nomenclature by referring to a spectrum Fraunhofer spectrum although it also contains spectral features from Earth's atmosphere) $I_0(\lambda)$ is chosen from one of the measurement spectra and the $dSCD(\alpha) = SCD(\alpha) - SCD_{ref}$ is obtained from the DOAS fit for each elevation angle α relative to the Fraunhofer reference. In the measurements reported here, the DOAS fit includes the cross sections listed in Table 2. By choosing references recorded shortly before and after the measurement spectrum, the influence of instrumental instabilities on the result was minimised as well as the influence of stratospheric absorbers.

3.2.1 The MAX-DOAS instrument during ANT XXVIII/1-2

The MAX-DOAS instrument operated during *Polarstern* cruise ANT XXVIII/1-2 consists of a telescope unit mounted on the deck of *Polarstern* on port side, which actively corrects for the roll movement of the ship, and a spectrometer unit with two temperature stabilised OMT (Optische Messtechnik GmbH) spectrometers ($f = 60$ mm, $|\Delta T| < 0.1\,°C$, $\Delta\lambda < 0.01$ nm), which have both been modified to minimise instrumental stray light (Lampel, 2014). Both spectrometers use back-thinned and peltier-cooled Hamamatsu S10141 CCD detectors in order to have a high quantum efficiency in the UV range. The optical resolution of the instrument during this campaign was 0.7 and 0.9 nm and it covered a spectral range from 277 to 413 nm and 390 to 617 nm, respectively. Spectra were recorded for 2 min each at seven elevation angles of 90° (zenith), 40, 20, 10, 5, 3, 1°, as long as solar zenith angles (SZA) were below 85°. Glyoxal data from this campaign were published in Mahajan et al. (2014).

3.2.2 The MAX-DOAS Instrument during M91

A description of the instrument operated during SOPRAN cruise M91 can be found in Großmann et al. (2013). The optical resolution of the instrument during this campaign was 0.45 nm. It covered a spectral range from 324 to 467 nm. The telescope elevation control unit actively compensated the ship's roll movement. Spectra were recorded for 1 min each at eight elevation angles of 90° (zenith), 40, 20, 10, 6, 4, 2, 1°, as long as SZA were ≤ 85°.

3.3 Spectral retrieval (MAX-DOAS)

The fit settings are summarised in Table 2 and example fits are shown in Fig. 5. As Fraunhofer reference spectra, the sum of the two 40° elevation angle spectra closest in time were used. Spectra recorded at a telescope elevation of 90° were not used as reference spectra, since they could have been influenced by direct sunlight during each of the MAX-DOAS campaigns close to the Equator. The wavelength calibration was performed using recorded mercury discharge lamp spectra. On ANT XXVIII/1-2 these were recorded automatically each night together with offset and dark-current spectra; during M91 they were recorded manually.

An additional intensity offset polynomial was used in the spectral evaluation to compensate for instrumental stray light, as described, e.g., in Peters et al. (2014).

Measurement errors of dSCDs are calculated as twice the DOAS fit error, according to Stutz and Platt (1996). This estimate is justified, because the standard deviation of the residual of the linear fit of H_2O / O_4 ratios at 363 and 477 nm shown in Fig. 6 amounts to 2.1 times the average DOAS fit error, and the residual spectra from the DOAS fit are dominated by noise in the UV. This estimate disregards possible systematic errors, but these are estimated to be small compared to the water vapour absorption ($< 2 \times 10^{-4}$) as the residual spectra are dominated by random noise (see Fig. 5).

For the water vapour absorption near 363 nm, the wavelength interval was chosen using the technique described in Vogel et al. (2013) on spectra recorded on 1 individual day (15 November 2011 at about 6° N, 17° W) of the ANT XXVIII/1-2 data set using the O_4 cross section at 298 K by Thalman and Volkamer (2013); for narrower wavelength ranges beginning above 345 nm and ending below 375 nm, lower H_2O dSCDs were observed during the day. However, the standard deviations of the H_2O dSCDs for these retrieval intervals are 5–6 $\times 10^{23}$ (uncorrected) as large as the mean dSCDs. For the larger fit intervals, the standard deviation is significantly smaller ($1–2 \times 10^{23}$), and the ratio of standard deviation of H_2O dSCDs and the average fit error is close to 2, as expected from Stutz and Platt (1996). For the broader fit intervals, the H_2O dSCD varies for fit intervals within 330–390 nm with a standard deviation of 16 % of mean H_2O dSCD. We thus estimate the error due to the choice of fit settings to be below 20 %. We assume that the small absorption structures of BrO and HCHO, which are not sufficiently constrained within fit intervals beginning above 345 nm, cause this effect and/or possible compensation of the relatively broad O_4 absorption by the DOAS polynomial. When including HONO in the DOAS analysis for this day with low-NO_2 concentrations and thus presumably low-HONO concentrations, enhanced HONO and H_2O dSCDs are observed simultaneously for fit intervals ending above 382 nm.

3.3.1 The blue spectral range

The effective centre of the respective absorptions of O_4 and H_2O can be calculated for each fit interval $[\lambda_1, \lambda_2]$ using

$$\lambda_m = \frac{1}{\int_{\lambda_1}^{\lambda_2} \sigma(\lambda) d\lambda} \int_{\lambda_1}^{\lambda_2} \lambda \sigma(\lambda) d\lambda. \tag{3}$$

In the wavelength interval from 452 to 499 nm, the effective centre of the water vapour absorptions of $\lambda_m^{H_2O} = 479$ nm is close to the effective centre of the O_4 absorptions at $\lambda_m^{O_4} = 476$ nm.

The fit range was chosen to have similar effective centres of absorptions of O_4 and H_2O in order to have comparable conditions for radiative transfer at both wavelengths.

HITEMP was chosen for the water vapour absorption cross section in the blue wavelength region. The differences in the blue wavelength region to HITRAN 2012 are negligible at a spectral resolution of 0.5 nm. HITEMP was chosen instead of POKAZATEL in the blue wavelength range, as already a couple of previous publications used this cross section in the blue wavelength range (see, e.g., Lampel et al., 2015b, and references therein). As described in Sect. 4.12 better agreement with observations was found for HITEMP than for POKAZATEL from 452 to 499 nm.

3.3.2 The near-UV spectral range

In the analysed wavelength interval of 340–380 nm the absorption structures of O_4 and H_2O are centred around $\lambda_m^{O_4} = 361$ nm and $\lambda_m^{H_2O} = 364$ nm.

As the observed OD in the fit ranges around 360 nm are small, except for the absorption of O_4 and the OD related to the Ring effect, it was necessary to include, in addition to the normal Ring spectrum, the temperature dependence of the Ring spectrum. The Ring spectrum itself compensates the measured apparent optical density due to inelastic scattering of sunlight on air molecules (Shefov, 1959; Grainger and Ring, 1962), which leads to an effective filling-in of Fraunhofer lines in the measured spectrum of scattered sunlight (e.g. Wagner et al., 2009, and references therein). The temperature dependence originates from the temperature dependence of the population of rotational states of the air molecules. It was calculated from the difference of Ring spectra $R(T)$ calculated at $T = 273$ K and $T = 243$ K using DOASIS (which is based on the work from Bussemer, 1993, parts of which can also be found in Platt and Stutz, 2008): $\Delta R / \Delta T = (R(T - \Delta T) - R(T)) / \Delta T$. The OD associated with the Ring spectrum temperature dependence amounts up to 5×10^{-4} for the M91 data set when using a Ring spectrum calculated at 273 K. For a Ring signal of 2.5×10^{25} (which is typical for MAX-DOAS observations), the Ring for a temperature difference of 30 K. We found that warmer effective Ring temperatures were found at low telescope elevation angles, which agrees with the lower tropospheric temperature

height profile. The temperature dependence of the derivative of the Ring spectrum with respect to temperature was found to be smaller than 0.5 %/1 K; therefore, it was sufficient to use one individual spectrum to linearise this effect.

The contribution of vibrational Raman scattering of air on measurements in this spectral range not only could be correlated to the size of the Ring effect but also agreed in its magnitude with the calculations given in Lampel et al. (2015a). Its effect on the results presented here was, however, negligible and was only consistently observed when co-adding spectra from more than four elevation sequences and for a rms of the resulting residuals of less than 1×10^{-4}. The effect of the wavelength dependence of the air mass factor (AMF) for the O_4 absorptions at 344, 361 and 380 nm was found to be negligible for the spectral retrieval of water vapour absorption in this spectral range.

4 Results and discussion

Starting with the largest absorption band below 380 nm listed in POKAZATEL at around 363 nm, we show first experimental evidence of water vapour absorption in the UV from LP-DOAS measurements (Sect. 4.1), which have the advantage of a well-defined light-path length. These are complemented by an even clearer detection of this absorption band by MAX-DOAS observations (Sect. 4.2). The magnitude of the absorption is quantified by comparison to water vapour absorption in the blue spectral range. From these results based on MAX-DOAS observations, a correction of the strength of the water vapour absorption band listed in POKAZATEL is derived. We then also estimated the magnitude of the weaker water vapour absorption bands to be at 335 nm (Sect. 4.6) and 373 nm (Sect. 4.7).

4.1 LP-DOAS: detection of water vapour absorption at 363 nm

Measurements between 22 August and 24 September 2015 were used for this analysis, when optimal instrumental performance could be guaranteed. Measurement spectra were co-added in order to reduce the rms of the residual in the UV fit interval to values of $1.5 \pm 0.3 \times 10^{-4}$ along the total light path of 6.12 km, which resulted in a time resolution of 2 h. This corresponds to an exposure time of about 15 min for each measurement spectrum. Due to the need to change the wavelength setting of the spectrometer between the different spectral windows around 440 and 360 nm, the time for each measurement sequence is shorter than the total time resolution.

A weak correlation of the water vapour absorption around 363 nm to the absorption at 442 nm was found with a correlation coefficient of $R^2 = 0.25$ (Fig. 4) for individual measurements. The rather weak correlation is due to the large individual measurement errors. This can be directly seen by the
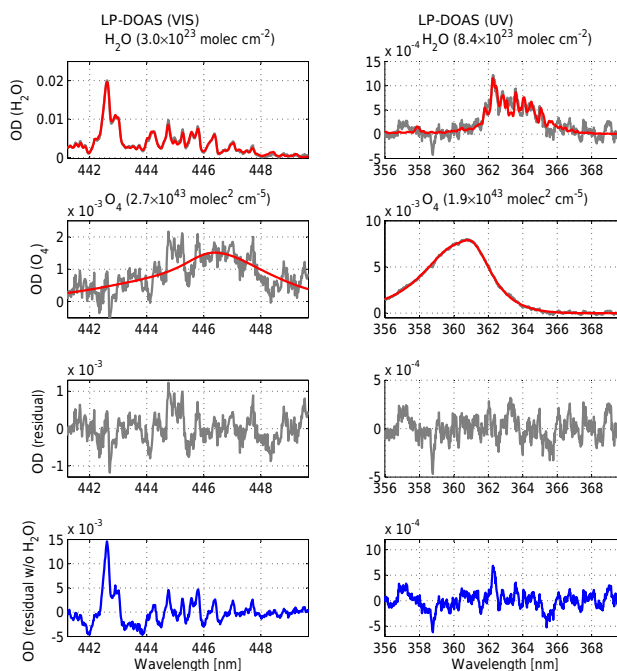

Figure 3. A LP-DOAS-fit result for the fitting intervals around 363 and 442 nm. The spectra were recorded on 29 August 2015 between 20:58 and 21:45 UTC. Top left panel: at 442 nm the H_2O dSCD $(3.0 \pm 0.04) \times 10^{23}$ molec cm^{-2} (O_4 dSCD $(2.7 \pm 0.6) \times 10^{43}$ molec^2 cm^{-5}). Top right panel: at 360 nm the H_2O dSCD $(8.4 \pm 0.6) \times 10^{23}$ molec cm^{-2} (O_4 dSCD $(1.85 \pm 0.03) \times 10^{43}$ molec^2 cm^{-5}).

large variations from one measurement to the next in the time series shown in Fig. 4 on the right. For daily averaged values the correlation amounts to $R^2 = 0.61$. Further co-adding of spectral measurement data could not reduce the measurement errors further, as systematic residual structures appear (see Fig. 3). Furthermore, large NO_2 concentrations of up to 20 ppb led to additional residual structures. Selecting measurement spectra according to the NO_2 concentration or rms did not improve the correlation.

As the measurement period was in late summer with temperatures between 9 and 36 °C and relative humidity between 20 and 96 % leading to a water vapour VMR between 0.4 and 1.3 % (5–16.5 g m^{-3}), low as well as high VMRs are not well represented in this data set. This increases the error in the correlation of water vapour column densities determined in both wavelength intervals (see Table 2). Linear regression yields a relative magnitude of the absorption near 363 nm of 2.31 ± 0.25 and an offset of $1.6 \pm 4.5 \times 10^{22}$ molec cm^{-2}. Fixing the offset to zero yields a scaling factor for the absorption cross section near 363 nm of 2.39 ± 0.05. This means, the POKAZATEL line lists underestimate the observed absorptions near 363 nm by a factor of 2.39. The measurement error will contribute significantly to the error of the scaling factor, as it is about 30 % of the maximally measured column
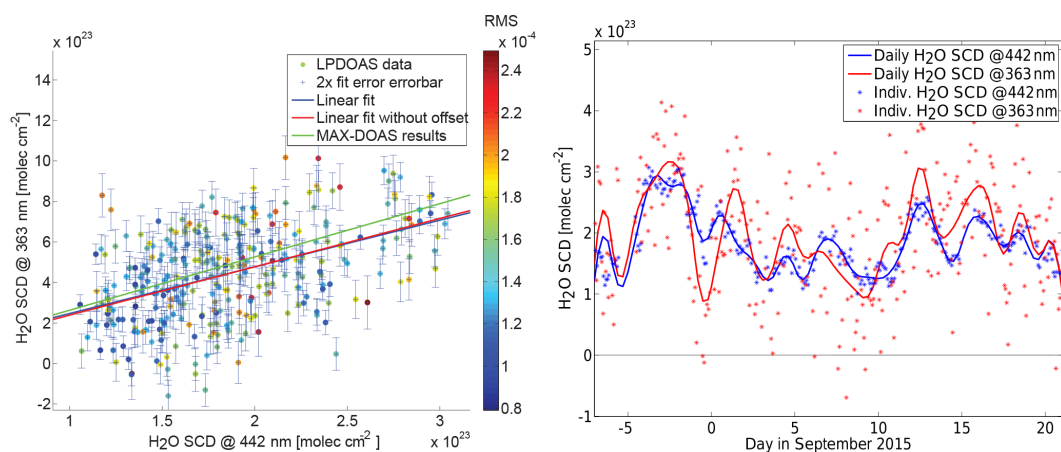
Figure 4. Left: correlation of H_2O slant column densities (SCDs) from LP-DOAS measurements near 363 and 442 nm. Also shown is the result from Table 3 line (1) from MAX-DOAS observations. Right: time series of H_2O column densities from LP-DOAS measurements near 363 and 442 nm. Values near 363 nm were corrected by the scaling factor determined from the correlation plot on the left.

density near 363 nm. Thus, we estimate the overall scaling factor from LP-DOAS measurements to be 2.4 ± 0.7.

4.2 MAX-DOAS: detection of water vapour absorption near 363 nm

The absorption of water vapour was detected at about 363 nm ($27\,548\,cm^{-1}$) in measurements from ANT XXVIII/1-2 and M91, using a fit interval from 340 to 380 nm ($26\,316$–$27\,548\,cm^{-1}$) according to Table 2. The maximum signal-to-noise ratio during both cruises (ratio between fitted H_2O dSCD and measurement error) were 14 and 10 (15 and 20, for 16 co-added elevation sequences). The corresponding dSCD values showed the typical separation for each elevation angle as observed for water vapour absorptions in the blue wavelength range. The corresponding spectra are shown in Fig. 5.

The retrieved water vapour dSCDs at 363 nm were compared to the 20 times stronger water vapour absorptions between 452 and 499 nm ($20\,040$–$22\,124\,cm^{-1}$) for the ANT XXVIII/1-2 data set. To correct for possible influences of varying radiative transfer conditions (which may result in different light-path lengths and thus different dSCDs), the H_2O dSCDs retrieved from both spectral windows were divided by the respective O_4 dSCD from the same fitting window. These fitting intervals were selected in a way that the wavelength of the main absorptions of O_4 and H_2O are at similar wavelengths. This needs to be done in order to have approximately the same radiative transfer properties for both absorbers (see Sect. 3.3.1). The wavelength ranges are listed in Table 2. The absorption of O_4 is an indicator for the light-path length, since the O_4 concentration is proportional to the square of the concentration of molecular oxygen, which has a well-defined and sufficiently constant concentration profile.

For Fig. 6, measurements at an elevation angle of 3–5° with an rms of less than 8×10^{-4} (UV) and 4×10^{-4} (VIS) were used; in addition, the error of the H_2O / O_4 ratio cal-

culated from the fit errors of both trace gases had to be below $5 \times 10^{-21}\,cm^3\,molec^{-1}$ (UV) and $3 \times 10^{-22}\,cm^3\,molec^{-1}$ (VIS). This implicitly removes all measurements with low-O_4 dSCDs, which is the case for fog and very low clouds. These conditions lead to different numbers of valid observations in Table 3 for different spectral retrieval settings.

The scale height of O_4 is 4 km, the scale height of water vapour is typically 2 km (Wagner et al., 2013). MAX-DOAS measurements of trace-gas dSCDs are most sensitive to the lowermost 2 km (e.g. Frieß et al., 2006). Thus, for a given surface volume-mixing ratio of water vapour, an almost constant ratio of H_2O and O_4 dSCD is expected. Figure 6 shows that this approximation is valid for the ANT XXVIII/1-2 measurements, as the correlation coefficients R^2 for the individual O_4 and H_2O dSCDs are smaller (0.81 and 0.74) than the correlation coefficient $R^2 = 0.89$ for their ratio.

However, the different profile shapes can introduce deviations, which were investigated by radiative transfer modelling using the Monte Carlo radiative transfer model McArtim (Deutschmann et al., 2011). Assuming different water vapour surface concentrations (0.1–3 %), water vapour scale heights of 1, 2 and 3 km, an aerosol layer with an extinction of 0, 0.2, 1, 2 and $10\,km^{-1}$, with a thickness of 1 and 3 km at an altitude of 0, 1, 2 and 3 km were the resulting simulated H_2O / O_4 dSCD ratios correlate for both wavelengths 363 and 477 nm, with an $R^2 = 0.98$ and a slope of 1.00 ± 0.02. The intercept was fixed to zero, elevation angles were 3, 5, 90° and 6480 individual simulations were performed. A significant systematic dependence of the ratios on ground albedo, solar zenith angle and relative azimuth angle was not observed, each of them resulting in less than a 1 % change of the simulated O_4 / H_2O ratio. Simulations with small O_4 dSCDs, which result in a large simulation error for the H_2O / O_4 dSCD ratio, were removed analogously to the measurements.
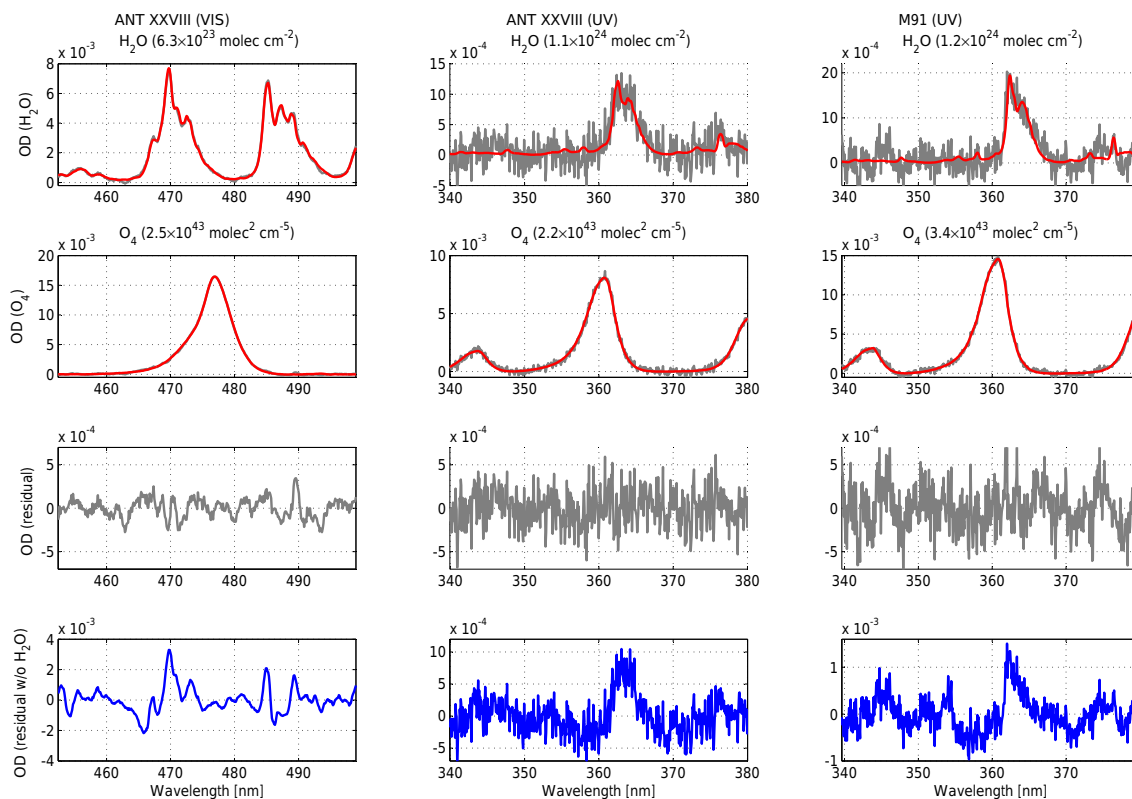
Figure 5. Fit results from ANT XXVIII/1-2 and M91 showing the detection of water vapour absorptions at 477 and 363 nm; in red, the modelled absorptions according to the cross sections listed in Table 2; in grey, the measured values. In blue, the residual is shown if no water vapour absorption was included in the fit. The fits from ANT XXVIII/1-2 use a spectrum (exposure time: 120 s; spectral resolution: 0.7 nm) from 16 November 2011 at 13:20 UTC at $3°59'06''$ N, $14°44'40''$ W at a telescope elevation angle of $3°$. At 477 nm the O_4 dSCD is $(2.47 \pm 0.01) \times 10^{43}$ molec^2 cm^{-5} and the H_2O dSCD $(6.27 \pm 0.06) \times 10^{23}$ molec cm^{-2}. At 360 nm the O_4 dSCD is $(2.18 \pm 0.04) \times 10^{43}$ molec^2 cm^{-5}, the H_2O dSCD $(1.13 \pm 0.16) \times 10^{24}$ molec cm^2. The fit from M91 is using one spectrum (exposure time: 60 s; spectral resolution: 0.45 nm) recorded on 5 December 2012, 19:44 UTC at $7°24'29''$ S, $81°30'18''$ W at a telescope elevation of $3°$. It shows an O_4 dSCD of $(3.43 \pm 0.02) \times 10^{43}$ molec^2 cm^{-5} and a H_2O dSCD of $(1.18 \pm 0.16) \times 10^{24}$ molec cm^{-2}. All fits used the O_4 cross section by Thalman and Volkamer (2013).

The Ångström exponent was varied using values of 0.0, 0.5 and 1.0 according to AERONET aerosol optical depth (AOD) measurements during ANT XXVIII/1 (Smirnov et al., 2009)[2]. The effect on the ratio was however also smaller than 1 %.

As for the measured data, the correlation of the simulated O_4 or H_2O dSCDs individually is significantly worse with $R^2_{O_4} = 0.74$ and $R^2_{H_2O} = 0.91$ compared to the correlation of their respective ratios. The slope of a linear polynomial fit to the O_4 dSCDs at 360 and 470 nm is similar to the observed values.

As seen from Fig. 6, the H_2O / O_4 dSCD ratios from ANT XXVIII/1-2 correlate well for the wavelength ranges around 360 nm and around 477 nm with an $R^2 = 0.89$. However, the absolute magnitude of the absorption cross section near

363 nm is underestimated by a factor of 2.6 ± 0.3 (see also Table 3).

In Fig. 2 the ratios of H_2O and O_4 dSCDs at $3°$ telescope elevation were converted to H_2O vertical column densities (VCDs) assuming a light path at ground level under normal conditions, a water vapour scale height of 2 km and using the correction factor of 2.6. Qualitatively the latitudinal variation of the ANT XXVIII/1-2 and GOME-2 data agree. For a quantitative comparison further radiative transfer modelling to obtain tropospheric water vapour profiles from the ship-based data would be needed.

The O_4 cross section is known to change its shape with changing temperature (Pfeilsticker et al., 2001; Thalman and Volkamer, 2013). As this effect could potentially introduce similar dependencies as the water vapour distribution, the spectral analysis was run in addition to the original analysis including two O_4 cross sections at 293 and 273 K. This changed the slope of the correlation shown in Fig. 6 by -10 % from 2.63 to 2.39 (see Table 3). In addition, an in-
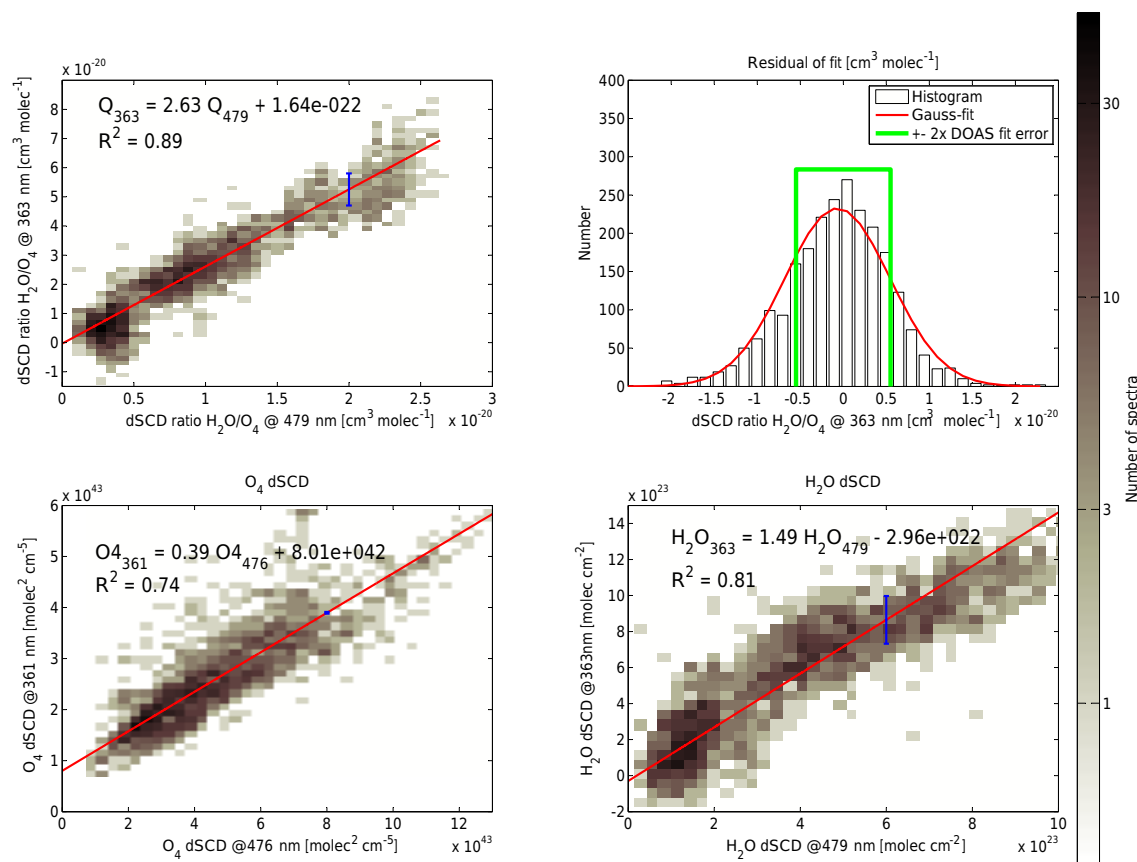
Figure 6. Top left panel: ratio of water vapour dSCD and O_4 dSCD at 363 and 479 nm for a telescope elevation angle of 3 and 5° during ANT XXVIII/1-2, using the O_4 cross section by Thalman and Volkamer (2013). Error bars represent typical measurement errors and are calculated from fit errors of both absorbers. Error bars for the ratios at 479 nm are omitted. They are more than 1 order of magnitude smaller than those at 363 nm. A ratio of 10^{-20} cm^3 molec^{-1} corresponds to an absolute water vapour-mixing ratio of 0.01 at ground level or a vertical column density of 5×10^{22} molec cm^{-2} or 15 kg H_2O m^{-2}, assuming a scale height of 2 km. Top right panel: the residual of the linear fit shows a Gaussian distribution and agrees with respect to its width of $\sigma = 6.12 \times 10^{-21}$ cm^3 molec^{-1} with the mean measurement error (2 times DOAS fit error, $2.75 \pm 0.92 \times 10^{-21}$ cm^3 molec^{-1}) obtained from the DOAS fit. The contribution of the statistical error of the linear fit is negligible. The individual correlations of H_2O and O_4 dSCDs are shown in the lower panels, which show individually smaller correlation coefficients than their respective ratios at 363 and 479 nm.

Table 3. Results from Fig. 6 to determine the relative magnitude of the water vapour absorption at 363 nm compared to 477 nm, using the HITEMP cross section for different retrieval settings using different O_4 cross sections. Values in brackets denote the error of the last digits of the respective value calculated from the error-weighted linear regression. For LP-DOAS measurements (see Sect. 4.1), the correlation was done for slant column densities (SCDs) instead of H_2O / O_4 dSCD ratios because the light path was constant. The offset (LP-DOAS) was, however, normalised by the mean O_4 dSCD at 360 nm in order to have comparable values. The systematic error of the slope was determined by using the typical relative measurement error of water vapour for measurements at a dSCD of 3×10^{23} molec cm^{-2} determined in the respective blue wavelength range.

	Type	O_4 cross section	R^2	Slope	Syst. error [%]	Offset [cm^3 molec^{-1}]	n
1	MAX-DOAS	Thalman 273 K	0.89	2.63(1)	8	$0.16(4) \times 10^{-21}$	2621
2	MAX-DOAS	Thalman 273 K free shift	0.88	2.61(1)	8	$0.34(4) \times 10^{-21}$	2634
3	MAX-DOAS	Thalman 273 + 293 K	0.83	2.39(1)	8	$7.25(5) \times 10^{-21}$	2562
4	MAX-DOAS	Hermans	0.86	2.62(1)	8	$4.22(4) \times 10^{-21}$	2630
5	MAX-DOAS	Greenblatt	0.84	2.55(1)	9	$21.1(1) \times 10^{-21}$	2183
6	MAX-DOAS	Greenblatt (shifted by 0.2 nm)	0.89	2.58(1)	11	$10.1(1) \times 10^{-21}$	2586
7	LP-DOAS	Thalman 293 K	0.25	2.31(25)	30	$1(3) \times 10^{-21}$	320

crease is observed for the offset of the linear fit, which should be ideally zero. Fixing the linear regression line for high water vapour content at the observed values, this increase in the offset of the linear fit corresponds to the observed change in the slope. We therefore conclude that the observed absorption structure is not caused by the temperature dependence of the O_4 absorption cross section, but indeed by water vapour absorption, as this offset is observed in polar regions, where almost no water vapour absorption is expected. Note that this offset is still small and amounts to 10 % (7.25×10^{-21} cm^3 molec^{-1}) of the observed maximum ratio of H_2O / O_4 dSCDs shown in Table 3.

A spectral shift of the O_4 literature cross section can effectively compensate parts of the water vapour absorption cross section at 363 nm. This is discussed in Sect. 4.5. However, stable results were even obtained when the shift of the set of literature cross sections was determined by the Levenberg–Marquardt algorithm of the DOAS fit, as shown in the second row in Table 3.

As seen from Table 3, the resulting slopes from Fig. 6 agree within their respective errors for different O_4 cross sections. The O_4 absorption by Greenblatt et al. (1990) shows a systematic shift for the absorption at 360 nm and was therefore analysed once with the original wavelength calibration and once shifted by 0.2 nm (used e.g. in Pinardi et al., 2013). The results of the shifted O_4 cross section include more measurements but still show a significant offset of the linear regression. The results using the Hermans et al. (1999) O_4 cross section seem more reliable, as more data points can be used and the offset of the slope is smaller. The most consistent results are obtained when using the O_4 cross section by Thalman and Volkamer (2013), showing a small offset and the highest correlation coefficient.

4.3 Differences using different dipole moment surfaces

The POKAZATEL line list employs the DMS from Lodi et al. (2011), while the POKAZATEL (CVR, core valence relativistic) line list employs the DMS from Lodi et al. (2008), using the same PES. This leads to significant differences in the intensities of the resulting line lists in the near-UV spectral region. The magnitude of the absorption between 362 and 365 nm in POKAZATEL (CVR) is on average 2.9 (ranges between 2.3 and 4.6) times larger than in POKAZATEL, and might therefore explain the observed discrepancy in the magnitude of the cross section shown in Sect. 4.2. However, the shape of the absorption band in the atmospheric measurements is significantly better predicted by POKAZATEL. Fitting POKAZATEL (CVR) to measured spectra from M91 leads to 20 % higher rms for the residual (see Fig. 7) at low-elevation angles. The additional absorption structures around 354 nm listed in POKAZATEL (CVR) are not found in observations (cf. Fig. 10). These findings are consistent with the spectral analysis of data from ANT XXVIII/1-2.
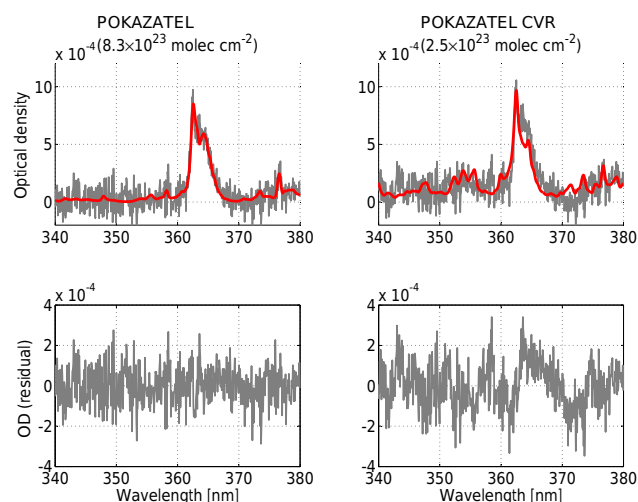

Figure 7. Two MAX-DOAS fits of the same measurement spectrum from M91 showing the detection of water vapour absorptions at 363 nm using two different DMSs (see Sect. 4.3). In order to reduce residual noise, the fit is using four spectra with a total exposure time of 240 s recorded on 22 December 2012, starting at 17:59 UTC at 15°31′ S, 75°36′ W at a telescope elevation of 3°. The POKAZATEL (CVR) line list shows a 20 % larger residual than POKAZATEL, whose shape fits the observed optical density better.

POKAZATEL (CVR) also predicts water vapour absorption between 330 and 360 nm, which should be above our detection limit. These could however not be identified for either of the two POKAZATEL nor the BT2 line lists during the M91 cruise (see also Sect. 4.6).

4.4 Comparison to other line lists

As shown in Fig. 1, other water vapour line lists also contain lines in the spectral range below 390 nm, which should be theoretically above typical detection limits of our measurements (often better than 10^{-4} along a light path of 10 km). However, in this spectral range BT2 and HITEMP are based on calculations only and have not yet been confirmed by laboratory or atmospheric measurements. The absorption at 380 nm should be clearly above the detection limit of the instrument used during M91, but as reported in Lampel et al. (2015b), it was not unambiguously found and showed inconsistencies. These two line lists show further absorption lines between 330 and 360 nm, which could also not be identified in Lampel et al. (2015b).

Fitting simultaneously a cross section based on POKAZATEL and a cross section based on HITEMP or BT2 to the measurements (M91), the optical density (from 340 to 380 nm) attributed to BT2 and HITEMP remained below (3 ± 12) and (2 ± 8) %, respectively, of the optical density of the water vapour absorption attributed to the POKAZATEL cross section. The optical density attributed to BT2 and HITEMP was (-1 ± 6) $\times 10^{-5}$ and (-1 ± 4) $\times 10^{-5}$, re-
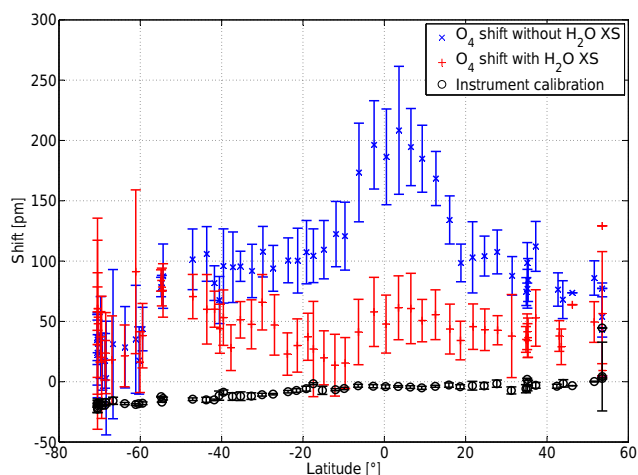
Figure 8. Error-weighted daily averaged DOAS-fit results for the shift of the O_4 cross section for measurements with a signal-to-noise ratio for the O_4 dSCD of more than 50. For this evaluation, the shift of the O_4 cross section was freely determined by the DOAS fit and not linked to the other absorption cross sections. Error bars denote the standard deviation during 1 day. The shift of the instrumental calibration was determined from the fit of the measured spectra to data from a convolved solar atlas.

spectively, while the POKAZATEL cross section showed absorptions of $(4.5 \pm 4.3) \times 10^{-4}$ for all spectra at all elevation angles of the M91 data set with an rms of the residual of less than 4×10^{-4}.

These findings demonstrate that the shape of the water vapour absorption appears to be better predicted in the POKAZATEL line list than in the BT2 and the HITEMP line list. For HITEMP this was expected, since HITEMP is partly based on BT2, but the individual line intensity cut-off leads to changes in absorption-band shape and the significantly smaller water vapour absorption cross section in HITEMP compared to BT2 as shown in Fig. 1.

4.5 Compensation of H$_2$O absorption by O$_4$ absorption near 363 nm

Since the water vapour absorption is found at the red flank of the O_4 absorption band at 361 nm, the absorption can be partly compensated by shifting the O_4 absorption band towards longer wavelengths. This effect is more clearly observed for the ANT XXVIII/1-2 data set than for the M91 data set, due to the lower spectral resolution, which seems to match better the widths of the spectral absorption structures of O_4.

When evaluating the ANT XXVIII/1-2 data set using the same settings as listed above in Table 2, but allowing for a spectral shift of the O_4 cross section by Thalman and Volkamer (2013), a systematic shift of the O_4 cross section of up to 0.20 nm relative to a Fraunhofer reference calibrated using the solar atlas of Chance and Kurucz (2010) is observed in

tropical regions (shown in Fig. 8). A systematic shift of the O_4 cross section of up to 0.15 nm relative to a freely shifting O_4 cross section from a fit including the POKAZATEL water vapour absorption cross section is observed. When the water vapour absorption is included, the free shift of the O_4 cross section shows a standard deviation of 0.035 nm for measurements with a signal-to-noise ratio of more than 50 for the O_4 dSCD. The instrument calibration shows a standard deviation of 0.007 nm due to a slow drift of 0.3 pm d^{-1}.

It was found that a small shift of O_4 with temperature (e.g. 0.05 nm as in Thalman and Volkamer (2013) from 273 to 293 K) cannot explain the apparent shift of the O_4 absorption when not considering the water vapour absorption.

As described in Beirle et al. (2013), a spectral shift can be linearised for small shifts by the derivative of the absorption cross section with respect to the wavelength using Taylor expansion. Turning the argument around, a correlation of the size of the absorption structure of water vapour and the product of O_4 absorption and spectral shift (from a DOAS fit where water vapour absorptions are not considered) is therefore expected. This correlation is found for ANT XXVIII/1-2 data with $R^2 = 0.89$ and a slope of $a_S = 6.78 \times 10^{18}$ nm molec cm^{-3}. For this instrument with a spectral resolution of 0.7 nm, it thus means effectively that a water vapour dSCD of $S_{H_2O} = 5 \times 10^{23}$ molec cm^{-2} and an O_4 dSCD of $S_{O_4} = 2.5 \times 10^{43}$ molec^2 cm^{-5} lead to a shift of the O_4 cross section by $a_S \cdot S_{H_2O}/S_{O_4} = 0.14$ nm, which was indeed observed in tropical regions as shown in Fig. 8. The change in overall O_4 dSCD is discussed in Sect. 4.11.

4.6 Upper limit for water vapour absorption at 335 nm

The water vapour absorption band at 335 nm in the POKAZATEL line list would amount to an OD of 1.2×10^{-4} for a water vapour dSCD of 4×10^{23} molec cm^{-2} at a spectral resolution of 0.5 nm.

Analogous to the procedure described in Sect. 4.2, the water vapour absorption band at 335 nm (fit range 332–358 nm) was compared to the water vapour absorption within the interval from 452 to 499 nm for the ANT XXVIII/1-2 measurements, divided by the dSCD of the respective O_4 absorption band. A clear correlation was not observed ($R^2 < 0.2$) due to too large fit errors to detect water vapour in the BrO–HCHO fit range (for fit settings see Table 2). The water vapour dSCD (at 335 nm) stayed below the average detection limit of 7×10^{23} molec cm^{-2}.

For the M91 MAX-DOAS measurements, the detection limit was reduced by co-adding 16 elevation sequences. However, the correlation of water vapour dSCDs at 335 and 442 nm was small ($R^2 = 0.2$) and the 2σ detection limit of 6.5×10^{23} molec cm^{-2} was only exceeded for 10 % of all spectra.

We therefore conclude that the predicted magnitude of the absorption at 335 nm is correct or overestimated, as we could not find it in our MAX-DOAS observations; if

the shape of the water vapour absorption is correctly predicted by POKAZATEL, the magnitude of the differential water vapour cross section from 332 to 358 nm at a spectral resolution of 0.45–0.70 nm is smaller than 2.5×10^{-28} cm^2 molec^{-1}.

4.7 Water vapour absorption around 376 nm

The literature values for the water vapour absorption cross sections based on POKAZATEL and BT2 (and thus also HITEMP) differ by about 1 order of magnitude in the spectral region between 370 and 380 nm (cf. Fig. 1). Using the M91 MAX-DOAS measurements the absorptions listed in BT2 could not be unambiguously identified or its predicted absorption shape did not match the observed absorptions. We therefore apply here the POKAZATEL line list on data from the M91 campaign.

We use a fit range from 370 to 386 nm and the settings for the water vapour absorption at 363 nm without considering the absorption cross section of O$_3$, HONO, BrO and HCHO. Co-added spectra based on four elevation sequences were used in order to reduce the average fit error to 2×10^{23} molec cm^{-2} (average rms of the residual: 1.1×10^{-4}). The water vapour dSCD was compared to the water vapour dSCD from 340 to 380 nm, retrieved in Sect. 4.2. The resulting correlation of dSCDs at 363 and 376 nm is significant with $R^2 = 0.6$ and a slope of 1.2 ± 0.3. A DOAS-fit result is shown in Fig. 9. As both absorption bands are at similar wavelengths and the absorptions are small, the difference in expected dSCDs introduced by differences in radiative transfer are negligible compared to the measurement error itself.

This shows that the water vapour absorptions at 376 nm is found in MAX-DOAS measurements and its magnitude is predicted in agreement with the absorption at 363 nm. It underestimates the absorption inferred from measurements by a factor of 3.1 ± 0.7.

4.8 Water vapour absorption below 330 nm

Du et al. (2013) reported significant water vapour absorptions of up to 2.94×10^{-24} cm^2 molec^{-1} at 330 nm and up to 2.19×10^{-24} cm^2 molec^{-1} at around 315 nm. Lampel et al. (2015b) could not confirm these findings and found upper limits for the differential absorption of water vapour from 332 to 370 nm of 3×10^{-27} cm^2 molec^{-1} from the M91 data set, which are 2 orders of magnitude smaller. Wilson et al. (2016) also could not confirm the values published by Du et al. (2013) between 325 and 420 nm. They estimated the water vapour absorption cross section at a spectral resolution of 0.5 nm to be less than 2×10^{-25} cm^2 molec^{-1}.

For a water vapour dSCD of 4×10^{23} molec cm^{-2}, the findings of Du et al. (2013) would result in differential optical depths around unity, which is unrealistic judging from observations of BrO and HCHO in the troposphere in wavelength intervals within 330–360 nm (see references listed in Vogel
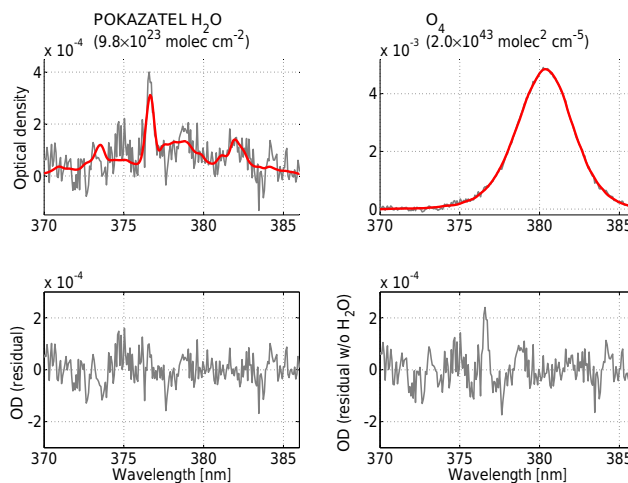

Figure 9. Fit result for the same MAX-DOAS spectrum as that used in Fig. 7 to show the water vapour absorption at 376 nm, which correlates for the M91 data set with $R^2 = 0.6$ and a slope of 1.2 ± 0.3, with the water vapour absorption at 363 nm. The measurement error of this individual fit amounts to 20 %.

et al., 2013 and Pinardi et al., 2013). The instrument operated during ANT XXVIII/1-2 covers a wider spectral range than in Lampel et al. (2015b), we therefore applied the BrO–HCHO fit settings from Table 2 to a fit interval from 310 to 350 nm. We used the water vapour dSCD determined from POKAZATEL at 363 nm of 4.3×10^{23} molec cm^{-2} for the spectrum from ANT XXVIII/1-2 shown in Fig. 5. For the calculation of the upper limit, we used conservatively only half of the value of the dSCD in order to account for the shorter light path at wavelengths between 310 and 350 nm. Polynomials with degree 0–2 were applied in the fit in order to account for broadband absorptions and scattering, and to estimate the dependence of the inferred upper limits on the degree of the DOAS polynomial. The polynomial could compensate for water vapour absorption if it is a rather broad absorption in this spectral region as suggested by Du et al. (2013). The resulting peak-to-peak (ptp) magnitudes of the residual are listed for an example measurement spectrum at 3° elevation angle in Table 4. To avoid unnecessary compensation of potential water vapour absorption by other absorbers, their dSCDs were determined using a DOAS polynomial of the third order, then the dSCDs of the trace gases in the fit were fixed to these values.

The resulting upper limits for the water vapour absorption cross section in the spectral range from 310 to 350 nm are thus 200–600 times smaller than the maximum cross section values measured by Du et al. (2013), and are 14–33 times smaller than the upper limit value presented in Wilson et al. (2016).

Table 4. Magnitude peak-to-peak (ptp) residual sizes and upper limits for water vapour absorption between 310 and 350 nm at a spectral resolution of 0.7 nm for different polynomial degrees of the DOAS polynomial.

Polynomial degree	ptp residual	Upper limit diff. H_2O XS cm^2 $molec^{-1}$
0	3.0×10^{-3}	14.0×10^{-27}
1	1.6×10^{-3}	5.4×10^{-27}
2	1.0×10^{-3}	4.6×10^{-27}

4.9 Estimation of the accuracy of the shape and wavelength calibration of the POKAZATEL H_2O cross section

The DOAS fit provides dSCDs as mentioned above, but also residual spectra.

These residual spectra are the difference between the modelled and the observed OD (cf. Fig. 5). In order to disentangle different contributions to the residual spectra, a multi-linear regression was performed based on the retrieved dSCDs (see Lampel et al., 2015a). This allows for the systematic identification of residual structures caused by each of the absorbers considered in the fit (cf. Table 2). However, since potential differences between modelled and observed absorptions can be compensated by any of the other absorbers, this information cannot be used to correct a given absorption cross section. It can though yield an estimate of the accuracy of the cross section.

For ANT XXVIII/1-2, the resulting spectrum from 340 to 380 nm, which correlates with the water vapour dSCD (shown in Fig. 10) has an rms of 1.7×10^{-28} cm^2 $molec^{-1}$ and a maximum peak-to-peak amplitude of 1.1×10^{-27} cm^2 $molec^{-1}$. The maximum magnitude of water vapour absorption cross section at 363 nm is 2.5×10^{-27} cm^2 $molec^{-1}$ for this spectral resolution (see Fig. 1). For M91, a residual structure at 344 nm is found, which could not be attributed to other absorbers and is correlated with the water vapour dSCD. The variation of humidity during M91 is significantly less than during ANT XXVIII/1-2; therefore, this structure could have been caused by any tropospheric absorber with a similar concentration height profile. As this residual structure is not observed for both data sets, we do not attribute it to water vapour absorption.

The maximum absorption of water vapour at 363 nm according to POKAZATEL seems to be re-shifted by 0.5 nm relative to the maximum absorption listed in BT2 (see inset in Fig. 1). To test if the wavelength of the water vapour absorption is correct, a spectral shift of the water vapour absorption was allowed; i.e. the shift was determined by the Levenberg–Marquardt algorithm of the DOAS fit. As the spectral resolution is higher, this was done for the M91 measurements.

The shift of the POKAZATEL water vapour absorption was found to agree with observations within 0.02 ± 0.06 nm (corresponding to 1.5 ± 4.6 cm^{-1}) for measurements exceeding a signal-to-noise ratio for the water vapour dSCD of 5 for the 16 elevation sequence co-added M91 data sets. This result is in agreement with the estimate of the precision of the PES by Polyansky et al. (2017), which was able to reproduce energy levels from laboratory measurements within about 0.1 cm^{-1} on average.

4.10 Further potential error sources

As the observed OD for water vapour absorption were small in the UV ($< 2\%$ for individual absorption lines at high spectral resolution), no saturation correction (Wenig et al., 2005) was applied during convolution of the line list for the spectral retrieval of MAX-DOAS data. The POKAZATEL line list does not provide line broadening parameters; therefore, the I_0 correction (Platt et al., 1997) also was not applied. This correction would have resulted in a change of the convolved cross section of less than 5 %.

In the visible (452–499 nm), the saturation effect for dSCD of 6×10^{23} $molec$ cm^{-2} amounts to less than 2 % change of the obtained dSCD.

4.10.1 Uncertainties of the H_2O literature cross sections in the blue wavelength range

Since we compared the UV absorptions of H_2O vapour to the values derived in the blue spectral region, the errors in the latter spectral region, which we analyse in the following, enter into the calculation of the total uncertainty of the UV absorption cross sections of H_2O.

The uncertainty of the absolute magnitude of water vapour cross section (HITEMP) in the blue wavelength from 452 to 499 nm is less than 15 %: The 6ν absorption band around 490 nm seems to be overestimated by (13 ± 3) % relative to the $6\nu + \delta$ absorption band around 470 nm when fitting the absorption bands separately analogously to Lampel et al. (2015b). This is one of the main reasons for the strongly structured fit residual in the visible fit range shown in Fig. 5.

The magnitude of the $6\nu + \delta$ absorption band around 470 nm agreed with the magnitude of the 7ν absorption band around 440 nm according to LP-DOAS measurements by Lampel et al. (2015b), for which in turn an agreement within 10 % with independent measurements of humidity and temperature was found in the same publication.

4.10.2 Uncertainties of the O_4 literature cross sections

For constant atmospheric water vapour content, water vapour and O_4 dSCDs from MAX-DOAS observations are typically well correlated because the bulk of the variations in the H_2O dSCD is due to variations in the path length. Therefore, it is important to disentangle potential problems of the water vapour absorption cross section and O_4 absorption cross
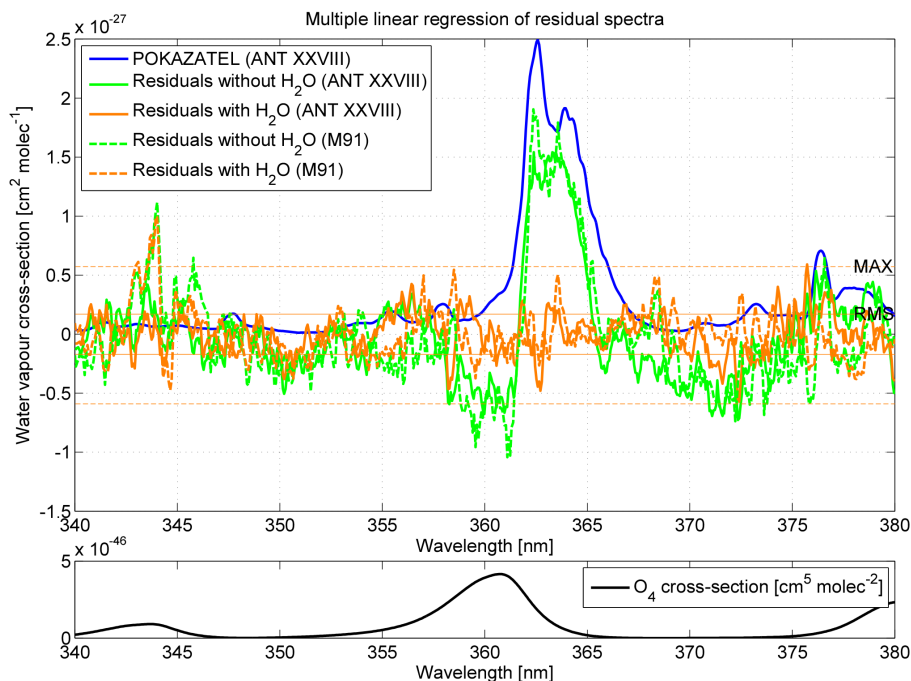
Figure 10. Using a multi-linear regression on the residual spectra from the campaigns ANT XXVIII/1-2 and M91, the water vapour dSCD-correlated residual structures were obtained. Negative values can be explained by compensation of the missing water vapour absorption structures by other absorbers included in the DOAS fit. The resulting spectrum, including water vapour absorption, yields an estimate on the accuracy of the convolved cross section.

section. The three available O_4 cross sections for the spectral range below 400 nm were published by Greenblatt et al. (1990), Hermans et al. (1999) and Thalman and Volkamer (2013). The POKAZATEL water vapour line list shows a local maximum at 363 nm (at a spectral resolution of 0.45 nm), which is at the slope of the O_4 absorption peak at 360.8 nm (see Fig. 1).

Differences in differential OD from 340 to 390 nm between different literature O_4 cross sections amount to up to 2×10^{-3} for a typical dSCD of O_4 of 4×10^{43} molec^2 cm^{-5}. This is larger than the OD of water vapour in this spectral range as listed in POKAZATEL. A systematic error in the respective O_4 cross section, which could lead to false apparent water vapour absorption, is expected to scale with the column density of O_4. It would thus result in a constant offset of the correlation of H_2O / O_4 ratios shown in Fig. 6. This was not observed. This also agrees with the observation that the wavelength dependence of the O_4 dSCDs was found to have no result on the water vapour dSCD at 363 nm. Thalman and Volkamer (2013) stated an absolute accuracy of 2–4 % for the their integrated O_4 absorption cross section at 361 and 476 nm.

For strong absorbers, the AMF of the observation also depends on the magnitude of the absorption itself (Marquard et al., 2000; Pukīte et al., 2010). However, for an optical density of O_4 at 360.8 nm of 2.5×10^{-3} we estimate a reduction of the effective light path by less than 1.3 %. This is an OD

of less than 3.5×10^{-4} and would result in a reduction of the apparent water vapour dSCD by 10 %. This effect would be smaller by a factor of 4 in tropical regions due to a smaller contribution of the O_4 absorption to the total optical depth. No correlation of the water vapour dSCDs at 363 nm with the square term of the O_4 absorption was found for the ANT XXVIII/1-2 data set.

The differences between the cross sections published by Thalman and Volkamer (2013), Greenblatt et al. (1990) and Hermans et al. (1999) did not allow to identify any systematic differences similar to the water vapour absorption, which could have pointed towards water vapour contamination during the acquisition of the cross section data.

As seen in Table 3, it was possible to observe good correlations for water vapour absorption at 363 nm and around 477 nm for all available O_4 literature cross sections. The smallest offset is observed when using the O_4 cross section by Thalman and Volkamer (2013). The best correlation coefficients R^2 are found for Thalman and Volkamer (2013) and Hermans et al. (1999).

Absolute maximum O_4 absorption cross section values differ for the three available cross sections at 293 K by less than 7 % at 360 nm and less than 5 % at 477 nm. This uncertainty could directly affect the H_2O / O_4 ratios listed in Table 3.

4.11 Influence on DOAS retrievals of other trace gases

Neglecting the water vapour absorption around 363 nm not only increases the fit errors of several DOAS trace-gas retrievals, but also could introduce a systematic bias in the trace-gas concentrations obtained. Trace-gas species, which are potentially influenced, are O_4, HONO, OClO and SO_2.

The effect may vary for different data sets, different DOAS fit intervals and different instrumental parameters such as the respective spectral resolution. Here the impact on trace-gas retrieval is investigated based on the M91 MAX-DOAS data set using the settings listed in Table 2. Only fit results with an initial rms of the fit residual of less than 4×10^{-4} were considered.

4.11.1 O_4 (340–380 nm)

For MAX-DOAS observations, the effective light-path length needs to be determined to convert observed slant column densities into concentrations of the respective trace gas. The absorption of the oxygen dimer O_4 can be used to infer information about atmospheric light paths (e.g. Wagner et al., 2002). Atmospheric aerosol extinction profiles can be estimated by constraining the input parameters of radiative transfer models to match the observed O_4 column densities. For MAX-DOAS measurements this approach has been described, e.g., in Wagner et al. (2004); Frieß et al. (2006). However, for some observations of scattered sunlight, the absorption of O_4 had to be corrected by a correction factor in order to explain the measured column densities as reported by (e.g. Wagner et al., 2009; Clémer et al., 2010; Irie et al., 2015). Clémer et al. (2010) estimated a correction factor value of 1.2–1.5 for modelled dSCD values to match observed dSCDs. The reason for this correction factor is so far unknown. However, for direct-sun DOAS measurements and measurements in the tropopause (Spinei et al., 2015) showed that a correction factor is not necessary to explain the measurements. Recently a possible explanation for a part of these previous observations was provided by Ortega et al. (2016): elevated aerosol layers in heights above 2 km, which affected the apparent O_4 dSCDs but could not be resolved from ground-based MAX-DOAS measurements due to their limited information content for aerosol extinction in these altitudes. Another reason for this correction factor could be an unaccounted tropospheric absorber, e.g. water vapour absorption.

To estimate the effect of water vapour absorption, the same evaluation for O_4 according to Table 2 was performed once with and once without the POKAZATEL water vapour absorption cross section. An increase in O_4 dSCD is observed when including the POKAZATEL water vapour absorption cross section in the DOAS evaluation.

Using the correction factor of 2.63 determined in Sect. 4.2, including the water vapour absorptions leads to an increase in O_4 dSCD per H_2O dSCD of $+(2.9 \pm 0.3) \times 10^{18}$ molec cm^{-3}, independent of the settings whether a shift and/or squeeze is allowed for the literature absorption cross sections.

For a typical H_2O dSCD of 4×10^{23} molec^{-2} in summer at mid-latitudes and a O_4 dSCD of 2.5×10^{43} molec^2 cm^{-5} (10 km light-path length), including the water vapour absorption, leads to an absolute increase of O_4 dSCD of 1.2×10^{42} molec^2 cm^{-5}, which corresponds to a change of $+5.0\%$.

Thus, the water vapour absorption at 363 nm cannot explain the correction factor for O_4 dSCDs introduced in various publications, it even increases the factor by $+5.0\%$ for measurements during summer in mid-latitudes.

4.11.2 HONO (337–375 nm)

Nitrous acid (HONO) is a key species in the atmospheric chemistry of urban air masses (e.g. Perner and Platt, 1979) because its photolysis leads to the production of OH radicals, the "detergent" of the atmosphere. Due to its high reactivity and fast daytime photolysis, HONO concentrations are low, in particular during daylight hours (Wong et al., 2012; Wang et al., 2016), and thus their measurements are difficult but can be performed, e.g., by absorption spectroscopy. If all relevant absorbers are accounted for, spectroscopic measurements have the advantage of being less affected by interferences, which were observed for wet chemical methods, e.g. LOPAP (e.g. Kleffmann and Wiesen, 2008). Therefore it is important to account for all possible absorbing trace-gas species in the respective wavelength range, e.g. 337–375 nm (Hendrick et al., 2014), in order to further reduce the detection limit and eliminate potential biases.

Adapting the wavelength range from Hendrick et al. (2014) and using the settings listed in Table 2, neglecting the water vapour absorption in the HONO fit has led to an decrease of HONO dSCDs. The decrease is clearly correlated to the water vapour dSCD and amounts per corrected H_2O dSCD to 1.4×10^{-9}. This corresponds to a H_2O dSCD of 4×10^{23} molec cm^{-2} to a negative bias of HONO dSCDs by 5.6×10^{14} molec cm^{-2}, which corresponds to a HONO surface volume-mixing ratio of 22 ppt along a light path of 10 km.

The rms decreases for this water vapour dSCD by 0.4×10^{-4} at a typical rms of 2.2×10^{-4}, which is a decrease of 18%.

This decrease of dSCDs explains negative HONO dSCDs around noon during M91, when not considering water vapour absorption.

At an elevation angle of 3°, we obtain a distribution of dSCDs around $(-3.9 \pm 2.4) \times 10^{14}$ molec cm^{-2} without including water vapour absorption. Including the water vapour absorption, the HONO dSCDs are distributed around $(1.0 \pm 2.3) \times 10^{14}$ molec cm^{-2}. During the cruise significant positive HONO dSCDs were observed close to NO_2 plumes from cities (HONO dSCDs of up to 2×10^{15} molec cm^{-2} at low telescope elevation angles), when the cruise track was close

Table 5. Impact on spectral retrievals estimated from DOAS evaluations with and without accounting for the water vapour absorption from POKAZATEL for the M91 MAX-DOAS data set (at a spectral resolution of 0.45 nm or 34 cm at 363 nm/27 548 cm). The typical difference was estimated for a water vapour dSCD of 4×10^{23} molec cm^{-2} along a 10 km long light path.

Trace gas	Wavelength (nm)	rms	Rel. change of dSCD per H$_2$O dSCD	Typ. diff.
O$_4$	340–380	−25 %	$+2.9 \times 10^{18}$ molec cm^{-3}	+5 %
HONO	337–375	−18 %	$+1.4 \times 10^{-9}$	+22 ppt
OClO	332–370	−20 %	$+3.1 \times 10^{-11}$	+0.5 ppt
SO$_2$	337–375	−20 %	-2.3×10^{-7}	−3.6 ppb

to the Peruvian coast. Therefore, a slightly positive average HONO dSCDs can be expected, but it is in agreement with zero within the standard deviation of the observed values. Filtering the results based on HONO dSCDs could have introduced a negative bias, as the observed HONO values are generally close to the respective detection limits. We therefore used the complete MAX-DOAS data set.

4.11.3 OClO (332–370 nm)

Stratospheric OClO has been observed in polar regions (e.g. Solomon et al., 1987; Kühl et al., 2008; Oetjen et al., 2011). Recently, OClO has also been observed in volcanic plumes (Bobrowski et al., 2007; Theys et al., 2014; Donovan et al., 2014; General et al., 2015; Gliß et al., 2015). All of these measurements were limited on one side of the retrieval interval close to 360 nm, potentially indicating unaccounted absorptions or erroneous O$_4$ cross sections.

Saiz-Lopez and von Glasow (2012) and references therein suggested that so far tropospheric OClO outside volcanic plumes has been observed only in polar regions with small absolute tropospheric water vapour content.

The 363 nm water vapour absorption band is located between two absorption bands of OClO and thus neglecting the water vapour absorption leads to an underestimation of OClO dSCDs and systematic residual structures.

Even when including water vapour absorption according to POKAZATEL, OClO was not positively identified during M91 (332–370 nm) above a 2σ detection limit of 1.6×10^{13} molec cm^{-2} at an elevation angle of 3°, the dSCDs showed a distribution around $(-0.9 \pm 8.0) \times 10^{12}$ molec cm^{-2}. Without correction for water vapour absorption, the dSCDs showed a distribution around $(-6.3 \pm 8.9) \times 10^{12}$ molec cm^{-2}.

Corrected by the scaling factor of 2.63 from Sect. 4.2, the increase in OClO dSCD per H$_2$O dSCD amounts to 3.08×10^{-11}. The difference in OClO is clearly correlated with the H$_2$O dSCD with $R^2 = 0.9$. This corresponds to a H$_2$O dSCD of 4×10^{23} molec cm^{-2} to an increase of OClO dSCD by 1.2×10^{13} molec cm^{-2}, which corresponds to a OClO surface volume-mixing ratio of 0.5 ppt along a light path of 10 km.
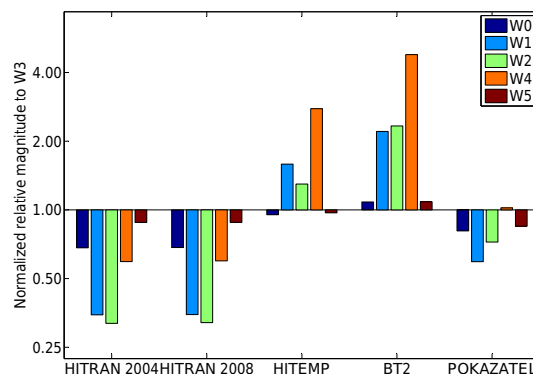

Figure 11. Comparison of different available water vapour cross section data in the blue spectral range, using different bands listed in Fig. 6. W3 was used as a respective reference in all cases and is therefore by definition unity. All magnitudes were normalised with respect to the rescaled HITEMP absorption cross section from Lampel et al. (2015b) to obtain relative magnitudes of each of the absorption bands W0, W1, W2, W4 and W5. A value of unity identifies good agreement with the relative magnitude of the absorption bands' sizes according to MAX-DOAS and LP-DOAS measurements presented in Lampel et al. (2015b).

4.11.4 Impact on the retrieval of other absorbers

In the spectral region below 360 nm, concentrations of HCHO and BrO can be retrieved. For HCHO systematic problems were discussed in Pinardi et al. (2013) and pointed towards uncertainties of the available O$_4$ cross sections. The absorptions listed within this fit range (336.5–359 nm) in BT2 are of similar magnitude to BrO concentrations for the lower troposphere as reported by Richter et al. (2002); Volkamer et al. (2015). POKAZATEL also lists lines here. So far, the absorption at 335 nm could not be unambiguously identified in measurements but can potentially have an impact on the spectral retrievals of tropospheric BrO and HCHO (see Sect. 4.6).

For very high column densities of SO$_2$, DOAS evaluation wavelength intervals above 340 nm can be used in order to minimise saturation effects due to large optical depths (Bobrowski et al., 2010; Hörmann et al., 2013). If such spectral evaluation schemes are applied to ground-based MAX-

Table 6. Integrated absorption in $[10^{-27}\,\mathrm{nm\,cm^2}]$ over each of the wavelength intervals W0–W5 for different sources of cross section data. Not only for the largest absorption structure W3 variations between the different compilations are seen, but especially integrated absorption values relative to W3 vary. The upper part of this table is adapted from Lampel et al. (2015b). The bold column marks the wavelength range, which was used as reference in Table 7 following the scheme from Lampel et al. (2015). These data are visualised in Fig. 11.

Dominating polyad name		8ν W0	$7\nu + \delta$ W1	W2	7ν **W3**	W4	$6\nu + \delta$ W5
Start of interval	[nm]	394.0	410.0	423.5	**434.0**	451.5	461.5
End of interval	[nm]	410.0	423.5	434.0	**451.5**	461.5	480.0
Source of cross section data	$[10^{-27}\,\mathrm{nm\,cm^2}]$			Integrated cross section			
HITRAN 2000		0.00	0.00	0.00	**69.02**	0.00	31.03
HITRAN 2004		13.62	3.11	0.89	**96.75**	0.87	42.25
HITRAN 2008 v2009	Rothman et al. (2009)	13.71	3.13	0.90	**97.07**	0.88	42.46
HITEMP	Rothman et al. (2010)	21.01	15.73	4.01	**106.90**	4.50	51.44
BT2	Barber et al. (2006)	26.05	23.84	7.86	**116.50**	8.46	62.67
HITEMP rescaled	Lampel et al. (2015b)	22.06	9.91	3.09	**106.90**	1.62	52.98
POKAZATEL	Polyansky et al. (2017)	15.98	5.26	2.00	**95.7**	1.48	40.26

Table 7. Measured relative absorption-band strengths for the different cross sections with respect to the absorption at W3 (the 7ν polyad; column in bold). Errors obtained from the linear regression are shown for the last digits in brackets. The relative DOAS fit errors are listed in Table 8. Results with typical DOAS fit errors of more than 25 % of the measured values were put in square brackets. MAX-DOAS values are corrected by the results of radiative transfer modelling (Lampel et al., 2015b).

Name		W0	W1	W2	**W3**	W4
Start of interval	[nm]	394.0	410.0	423.5	**434.0**	451.5
End of interval	[nm]	410.0	423.5	434.0	**451.5**	461.5
POKAZATEL		1.2605(6)	1.7052(13)	[0.8135(41)]	**1**	[2.1270(81)]

DOAS measurements also using low telescope elevation angles for locations with high absolute water vapour concentrations, water vapour absorption might need to be also considered in the spectral evaluation of SO_2. We estimated the impact using the HONO (337–375 nm) fit settings with the additional SO_2 absorption cross section from Vandaele et al. (2009) in Table 5. The overall change in dSCD was of the same magnitude as the fit error (see Table 5).

4.12 MAX-DOAS: relative water vapour absorption-band strengths in the blue spectral range

The consistency of the POKAZATEL line list with other line lists and measured absorption was checked in analogy to Lampel et al. (2015b) in the blue spectral range for MAX-DOAS observations. The relative absorption strength relative to the much stronger absorption band around 442 nm, which is called W3 here, was determined for the POKAZATEL water vapour line list. The different wavelength intervals are listed in Table 6. The same MAX-DOAS data set (M91) and the same settings as described in Lampel et al. (2015b) were applied. The magnitude of the absorptions W0

and W1 are underestimated compared to MAX-DOAS observations, leading to the observation of water vapour dSCDs, which are 26 %(W0) and 71 %(W1) larger than the dSCDs observed simultaneously for the stronger absorption W3. The results are shown in Fig. 7 and Table 8.

Overall, POKAZATEL predicts the integrated absorption cross sections in the blue spectral range to the 480 nm range better than previous versions of HITRAN and BT2, as seen from Table 6 and summarised in Fig. 11. It was however not used as a reference cross section in the blue wavelength range, as HITEMP (and HITRAN2012) reproduced the observed water vapour absorptions in the blue fit interval (452–499 nm) significantly better. These differences, which are also seen from Fig. 1, will require further investigation, as they do not only involve a difference of the overall absorption strength of both bands near 470 and 490 nm, but also differences in the shape of the absorption bands were observed between HITEMP and POKAZATEL (see also Sect. 4.10.1).

Table 8. Typical relative DOAS fit errors in fitting windows W0–W4 at a water vapour dSCD in W3 of 4×10^{23} molec cm^{-2} for an individual spectrum integrated over 60 s. Values are given in % and are corrected by the relative magnitudes given in Table 7.

[%]		W0	W1	W2	**W3**	W4
Start of interval	[nm]	394.0	410.0	423.5	**434.0**	451.5
End of interval	[nm]	410.0	423.5	434.0	**451.5**	461.5
POKAZATEL	MAX-DOAS	4	6	40	**0.8**	29

5   Conclusions

The water vapour absorption structure predicted from calculations for wavelengths around 363 nm by Polyansky et al. (2017) was found for the first time in two different MAX-DOAS measurement data sets of tropospheric air masses with optical depths of up to 2×10^{-3} at a spectral resolution of 0.45–0.7 nm. Additionally, it was observed for the first time in LP-DOAS observations. Until now, to our knowledge these absorptions were neither experimentally verified nor considered in the spectral analysis of DOAS observations.

Comparing the strengths of the UV absorption lines of water vapour to the water vapour absorptions listed in HITEMP between 452 and 499 nm showed that the absorptions are indeed caused by water vapour, and that the cross section calculated from the data provided by Polyansky et al. (2017) underestimates the measured absorption by a factor of 2.6 ± 0.5. For MAX-DOAS, the different light-path lengths in the two different wavelength windows were corrected by normalisation with the respective O$_4$ dSCD in the same wavelength interval. The water vapour absorption feature at 363 nm in MAX-DOAS measurements was identified and shown to be independent of the chosen literature value of the O$_4$ absorption cross section; i.e. it was found to be at a similar magnitude for all three available O$_4$ literature absorption cross sections. It was also independent of the temperature-induced broadening of the O$_4$ cross section.

In contrast, a slight spectral shift of the O$_4$ reference spectrum could have compensated in previous evaluations (not including the 363 nm H$_2$O absorption) for the water vapour absorption, which is located on a slope of the O$_4$ absorption (Sect. 4.5). This apparent shift might have lead to wavelength calibration corrections of O$_4$ literature cross sections in previous publications for individual campaigns with relatively constant H$_2$O / O$_4$ dSCD ratios.

Other predicted water vapour absorption features at 335 nm could not be unambiguously identified in the measurements as these did not exceed the respective detection limits. The absorption structure at 377 nm was slightly above the detection limit and was found to correlate with the water vapour absorption at 363 nm.

The identified water vapour absorption at 363 nm can have a significant impact on the retrieval of trace gases, which absorb in the same wavelength range, namely O$_4$, HONO, OClO and SO$_2$. For measurement locations with high abso-lute water vapour concentrations, consideration of the water vapour absorption at 363 nm, if included in the spectral analysis of MAX-DOAS measurements, will lead to a reduction of measurement errors and will thus lower the overall limit of detection. We showed that neglecting this absorption introduces systematic biases in their spectral analysis.

During M91, for O$_4$ dSCDs an increase of about 5 % was observed when including the additional absorption in the DOAS analysis. Thus, the water vapour absorption cannot explain the much larger correction factor for O$_4$ dSCDs introduced in various publications (it rather increases the observed discrepancies).

For HONO the water vapour absorption explains negative HONO dSCDs of several 10^{14} molec cm^{-2} for mid-latitude absolute water vapour volume-mixing ratios. Negative HONO dSCD at low-elevation angles were often observed around noon during the SOPRAN M91 campaign in the Peruvian upwelling when not considering water vapour absorption. In the same way negative OClO dSCDs in MAX-DOAS observations at low-elevation angles of around -1×10^{13} molec cm^{-2} during M91 could also be linked to water vapour absorption at 363 nm.

Future DOAS evaluations encompassing the spectral range around 363 nm will require one to include these water vapour absorption features, if they aim at residual spectra with an rms of less than 4×10^{-4} or try to fit absorbers with measurement errors corresponding to optical densities of less than 1×10^{-3} in mid-latitude to tropical regions.

The predictions of POKAZATEL do not yield complete agreement with the observed absorption features. While, as discussed above, this line list should give very accurate line positions, the situation regarding absorption intensities is more problematic. This is indeed observed in the measurements presented here, as the position of the absorption is found to be accurate (shift of 0.02 ± 0.06 nm, or 1.5 ± 4.6 cm^{-1}), while the magnitude of the observed absorption bands differs relative to each other. This was before also observed in the blue spectral range by Lampel et al. (2015b). While the ab initio dipole moment calculations of Lodi et al. (2011) cover an appropriate range of geometries and are expected to be accurate, using them to construct a reliable DMS is not straightforward. A number of studies (Schwenke and Partridge, 2000; Lodi et al., 2008; Tennyson, 2014) have shown that it is difficult to produce analytic fits,

which correctly reproduce the intensity of weak transitions. Here we are dealing with very weak water absorptions on the margins of detectability. For this reason we performed some test calculations using the POKAZATEL methodology but utilising the CVR DMS of Lodi et al. (2008). The results shown in Sect. 4.3 indicate that this DMS (Lodi et al., 2008) could explain the systematic underestimation of the magnitude of water vapour absorption, but probably do not predict the spectral shape of the absorption peak as accurately as POKAZATEL. Further work is required on the precise representation of the ab initio DMS to try to resolve these problems. Studies should also be performed to obtain a more reliable representation of the water dipole moment for the purpose of predicting absorption intensities in the near-UV. Laboratory studies on this problem would also be very helpful.

The values for the absorption cross section of water vapour in the UV range reported by Du et al. (2013) cannot be confirmed. We derived upper limits, which are at least 2 orders of magnitude smaller in the spectral range from 310 to 370 nm.

6 Data availability

The raw spectral data (more than 700MB of binary data) of the MAX-DOAS and LP-DOAS measurements can be obtained on request from the authors.

References

Bange, H.: Surface Ocean – Lower Atmosphere Study (SOLAS) in the upwelling region off Peru – Cruise No.M91, DFG-Senatskommission fuer Ozeanographie, METEOR-Berichte, 91, 69 pp., doi:10.2312/cr_m91, 2013.

Barber, R. J., Tennyson, J., Harris, G. J., and Tolchenov, R. N.: A high-accuracy computed water line list, Mon. Not. R. Astron. Soc., 368, 1087–1094, doi:10.1111/j.1365-2966.2006.10184.x, 2006.

Beirle, S., Sihler, H., and Wagner, T.: Linearisation of the effects of spectral shift and stretch in DOAS analysis, Atmos. Meas. Tech., 6, 661–675, doi:10.5194/amt-6-661-2013, 2013.

Bobrowski, N., von Glasow, R., Aiuppa, A., Inguaggiato, S., Louban, I., Ibrahim, O. W., and Platt, U.: Reactive halogen chemistry in volcanic plumes, J. Geophys. Res.-Atmos., 112, D06311, doi:10.1029/2006JD007206, 2007.

Bobrowski, N., Kern, C., Platt, U., Hörmann, C., and Wagner, T.: Novel SO2 spectral evaluation scheme using the 360–390 nm wavelength range, Atmos. Meas. Tech., 3, 879–891, doi:10.5194/amt-3-879-2010, 2010.

Bogumil, K., Orphal, J., Homann, T., Voigt, S., Spietz, P., Fleischmann, O., Vogel, A., Hartmann, M., Bovensmann, H., Frerik, J., and Burrows, J.: Measurements of Molecular Absorption Spectra with the SCIAMACHY Pre-Flight Model: Instrument Characterization and Reference Data for Atmospheric Remote-Sensing in the 230–2380 nm Region, J. Photochem. Photobiol. A., 157, 167–184, 2003.

Boyarkin, O. V., Koshelev, M. A., Aseev, O., Maksyutenko, P., Rizzo, T. R., Zobov, N. F., Lodi, L., Tennyson, J., and Polyansky, O. L.: Accurate bond dissociation energy of water determined by triple-resonance vibrational spectroscopy and ab initio calculations, Chem. Phys. Lett., 568–569, 14–20, 2013.

Bussemer, M.: Der Ring- Effekt: Ursachen und Einfluß auf die spektroskopische Messung stratosphärischer Spurenstoffe, Diploma thesis, Heidelberg University, Heidelberg, Germany, available at: http://katalog.ub.uni-heidelberg.de/titel/59803137 (last access: 18 January 2017), 1993.

Chance, K. and Kurucz, R.: An improved high-resolution solar reference spectrum for earth's atmosphere measurements in the ultraviolet, visible, and near infrared, J. Quant. Spectrosc. Ra., 111, 1289–1295, doi:10.1016/j.jqsrt.2010.01.036, special Issue Dedicated to Laurence S. Rothman on the Occasion of his 70th Birthday, 2010.

Chance, K. and Orphal, J.: Revised ultraviolet absorption cross sections of H2CO for the HITRAN database, J. Quant. Spectrosc. Ra., 112, 1509–1510, doi:10.1016/j.jqsrt.2011.02.002, 2011.

Clémer, K., Van Roozendael, M., Fayt, C., Hendrick, F., Hermans, C., Pinardi, G., Spurr, R., Wang, P., and De Mazière, M.: Multiple wavelength retrieval of tropospheric aerosol optical properties from MAXDOAS measurements in Beijing, Atmos. Meas. Tech., 3, 863–878, doi:10.5194/amt-3-863-2010, 2010.

Császár, A. G., Mátyus, E., Lodi, L., Zobov, N. F., Shirin, S. V., Polyansky, O. L., and Tennyson, J.: Ab initio prediction and partial characterization of the vibrational states of water up to dissociation, J. Quant. Spectrosc. Ra., 111, 1043–1064, 2010.

Deutschmann, T., Beirle, S., Friess, U., Grzegorski, M., Kern, C., Kritten, L., Platt, U., Prados-Roman, C., Pukīte, J., Wagner, T., Werner, B., and Pfeilsticker, K.: The Monte Carlo atmospheric radiative transfer model McArtim: Introduction and validation of Jacobians and 3D features, J. Quant. Spectrosc. Ra., 112, 1119–1137, doi:10.1016/j.jqsrt.2010.12.009, 2011.

Donovan, A., Tsanev, V., Oppenheimer, C., and Edmonds, M.: Reactive halogens (BrO and OClO) detected in the plume of Soufrière Hills Volcano during an eruption hiatus, Geochem. Geophy. Geosy., 15, 3346–3363, doi:10.1002/2014GC005419, 2014.

Du, J., Huang, L., Min, Q., and Zhu, L.: The influence of water vapor absorption in the 290–350 nm region on solar radiance: Laboratory studies and model simulation, Geophys. Res. Lett., 40, 4788–4792, doi:10.1002/grl.50935, 2013.

Dupré, P., Gherman, T., Zobov, N. F., Tolchenov, R. N., and Tennyson, J.: Continuous-wave cavity ringdown spectroscopy of the 8ν polyad of water in the 25 195–25 340 cm range, J. Chem. Phys., 123, 154 307, 2005.

Eger, P.: Improving Long-Path DOAS measurements with a Laser Driven Light Source and a new fibre configuration, Masters thesis, Institut für Umweltphysik, Universität Heidelberg, 2014.

Fleischmann, O.: New ultraviolet absorption cross-sections of BrO at atmospheric temperatures measured by time-windowing Fourier transform spectroscopy, J. Photoch. Photobio. A, 168, 117–132, 2004.

Frieß U., Monks, P. S., Remedios, J. J., Rozanov, A., Sinreich, R., Wagner, T., and Platt, U.: MAX-DOAS O_4 measurements: A new technique to derive information on atmospheric aerosols: 2. Modeling studies, J. Geophys. Res., 111, D14203, doi:10.1029/2005JD006618, 2006.

General, S., Bobrowski, N., Pöhler, D., Weber, K., Fischer, C., and Platt, U.: Airborne I-DOAS measurements at Mt. Etna: BrO and {OClO} evolution in the plume, J. Volcanol. Geoth. Res., 300, 175–186, doi:10.1016/j.jvolgeores.2014.05.012, 2015.

Gliß, J., Bobrowski, N., Vogel, L., Pöhler, D., and Platt, U.: OClO and BrO observations in the volcanic plume of Mt. Etna – implications on the chemistry of chlorine and bromine species in volcanic plumes, Atmos. Chem. Phys., 15, 5659–5681, doi:10.5194/acp-15-5659-2015, 2015.

Grainger, J. and Ring, J.: Anomalous Fraunhofer line profiles, Nature, 193, 762 pp., 1962.

Greenblatt, G. D., Orlando, J. J., Burkholder, J. B., and Ravishankara, A. R.: Absorption Measurements of Oxygen between 330 and 1140 nm, J. Geophys. Res., 95, 18577–18582, 1990.

Großmann, K., Frieß, U., Peters, E., Wittrock, F., Lampel, J., Yilmaz, S., Tschritter, J., Sommariva, R., von Glasow, R., Quack, B., Krüger, K., Pfeilsticker, K., and Platt, U.: Iodine monoxide in the Western Pacific marine boundary layer, Atmos. Chem. Phys., 13, 3363–3378, doi:10.5194/acp-13-3363-2013, 2013.

Hendrick, F., Müller, J.-F., Clémer, K., Wang, P., De Mazière, M., Fayt, C., Gielen, C., Hermans, C., Ma, J. Z., Pinardi, G., Stavrakou, T., Vlemmix, T., and Van Roozendael, M.: Four years of ground-based MAX-DOAS observations of HONO and

NO_2 in the Beijing area, Atmos. Chem. Phys., 14, 765–781, doi:10.5194/acp-14-765-2014, 2014.

Hermans, C., Vandaele, A. C., Carleer, M., Fally, S., Colin, R., Jenouvrier, A., Coquart, B., and Mérienne, M.-F.: Absorption Cross-Sections of Atmospheric Constituents: NO_2, O_2, and H_2O, Environ. Sci. Pollut. R., 6, 151–158, doi:10.1007/BF02987620, 1999.

Hermans, C., Vandaele, A., Fally, S., Carleer, M., Colin, R., Coquart, B., Jenouvrier, A., and Merienne, M.-F.: Absorption cross-section of the collision-induced bands of oxygen from the UV to the NIR, in: Weakly interacting molecular pairs: unconventional absorbers of radiation in the atmosphere, edited by: Camy-Peyret, C. and Vigasin, A. A., 193–202, Springer Netherlands, Dordrecht, 2003.

Hönninger, G. and Platt, U.: Observations of BrO and its vertical distribution during surface ozone depletion at Alert, Atmos. Environ., 36, 2481–2489, 2002.

Hönninger, G., von Friedeburg, C., and Platt, U.: Multi axis differential optical absorption spectroscopy (MAX-DOAS), Atmos. Chem. Phys., 4, 231–254, doi:10.5194/acp-4-231-2004, 2004.

Hörmann, C., Sihler, H., Bobrowski, N., Beirle, S., Penning de Vries, M., Platt, U., and Wagner, T.: Systematic investigation of bromine monoxide in volcanic plumes from space by using the GOME-2 instrument, Atmos. Chem. Phys., 13, 4749–4781, doi:10.5194/acp-13-4749-2013, 2013.

Irie, H., Nakayama, T., Shimizu, A., Yamazaki, A., Nagai, T., Uchiyama, A., Zaizen, Y., Kagamitani, S., and Matsumi, Y.: Evaluation of MAX-DOAS aerosol retrievals by coincident observations using CRDS, lidar, and sky radiometer in Tsukuba, Japan, Atmos. Meas. Tech., 8, 2775–2788, doi:10.5194/amt-8-2775-2015, 2015.

Jacquinet-Husson, N., Scott, N., Chédin, A., Crépeau, L., Armante, R., Capelle, V., Orphal, J., Coustenis, A., Boonne, C., Poulet-Crovisier, N., Barbe, A., Birk, M., Brown, L. R., Camy-Peyret, C., Claveau, C., Chance, K., Christidis, N., Clerbaux, C., Coheur, P. F., Dana, V., Daumont, L., De Backer-Barilly, M. R., Di Lonardo, G., Flaud, J. M., Goldman, A., Hamdouni, A., Hess, M., Hurley, M. D., Jacquemart, D., Kleiner, I., Köpke, P., Mandin, J. Y., Massie, S., Mikhailenko, S., Nemtchinov, V., Nikitin, A., Newnham, D., Perrin, A., Perevalov, V. I., Pinnock, S., Régalia-Jarlot, L., Rinsland, C. P., Rublev, A., Schreier, F., Schult, L., Smith, K. M., Tashkun, S. A., Teffo, J. L., Toth, R. A., Tyuterev, V. G., Vander Auwera, J., Varanasi, P., and Wagner, G.: The GEISA spectroscopic database: Current and future archive for Earth and planetary atmosphere studies, J. Quant. Spectrosc. Ra., 109, 1043–1059, 2008.

Kattner, G.: The expedition of the research vessel "Polarstern" to the Antarctic in 2011/12 (ANT-XXVIII/2), available at: http://hdl.handle.net/10013/epic.39675 (last access: 18 January 2017), 2012.

Kleffmann, J. and Wiesen, P.: Technical Note: Quantification of interferences of wet chemical HONO LOPAP measurements under simulated polar conditions, Atmos. Chem. Phys., 8, 6813–6822, doi:10.5194/acp-8-6813-2008, 2008.

Kraus, S.: DOASIS – A Framework Design for DOAS, Dissertation, Heidelberg University, 2006.

Kühl, S., Pukīte, J., Deutschmann, T., Platt, U., and Wagner, T.: SCIAMACHY limb measurements of NO_2, BrO and OClO. Retrieval of vertical profiles: Algorithm, first results, sensitiv-

ity and comparison studies, Adv. Space Res., 42, 1747–1764, doi:10.1016/j.asr.2007.10.022, 2008.

Lampel, J.: Measurements of reactive trace gases in the marine boundary layer using novel DOAS methods, Dissertation, Institut für Umweltphysik, Heidelberg University, available at: http://www.ub.uni-heidelberg.de/archiv/17394 (last access: 18 January 2017), 2014.

Lampel, J., Frieß, U., and Platt, U.: The impact of vibrational Raman scattering of air on DOAS measurements of atmospheric trace gases, Atmos. Meas. Tech., 8, 3767–3787, doi:10.5194/amt-8-3767-2015, 2015a.

Lampel, J., Pöhler, D., Tschritter, J., Frieß, U., and Platt, U.: On the relative absorption strengths of water vapour in the blue wavelength range, Atmos. Meas. Tech., 8, 4329–4346, doi:10.5194/amt-8-4329-2015, 2015b.

Lodi, L. and Tennyson, J.: Line lists for $H_2^{18}O$ and $H_2^{17}O$ based on empirically-adjusted line positions and ab initio intensities, J. Quant. Spectrosc. Ra., 113, 850–858, 2012.

Lodi, L., Tolchenov, R. N., Tennyson, J., Lynas-Gray, A., Shirin, S. V., Zobov, N. F., Polyansky, O. L., Császár, A. G., van Stralen, J. N., and Visscher, L.: A new ab initio ground-state dipole moment surface for the water molecule, J. Chem. Phys., 128, 044304, doi:10.1063/1.2817606, 2008.

Lodi, L., Tennyson, J., and Polyansky, O. L.: A global, high accuracy ab initio dipole moment surface for the electronic ground state of the water molecule, J. Chem. Phys., 135, 034113, doi:10.1063/1.3604934, 2011.

Mahajan, A. S., Prados-Roman, C., Hay, T. D., Lampel, J., Pöhler, D., Großmann, K., Tschritter, J., Frieß, U., Platt, U., Johnston, P., Kreher, K., Wittrock, F., Burrows, J. P., Plane, J. M., and Saiz-Lopez, A.: Glyoxal observations in the global marine boundary layer, J. Geophys. Res.-Atmos., 119, 6160–6169, doi:10.1002/2013JD021388, 2014.

Maksyutenko, P., Muenter, J. S., Zobov, N. F., Shirin, S. V., Polyansky, O. L., Rizzo, T. R., and Boyarkin, O. V.: Approaching the full set of energy levels of water, J. Chem. Phys., 126, 241101–241101, 2007.

Maksyutenko, P., Grechko, M., Rizzo, T. R., and Boyarkin, O. V.: State-resolved spectroscopy of high vibrational levels of water up to the dissociative continuum, Philos. T. R. Soc. A, 370, 2710–2727, 2012.

Marquard, L. C., Wagner, T., and Platt, U.: Improved air mass factor concepts for scattered radiation differential optical absorption spectroscopy of atmospheric species, J. Geophys. Res., 105, 1315–1327, 2000.

Myhre, G., Shindell, D., Bréon, F.-M., Collins, W., Fuglestvedt, J., Huang, J., Koch, D., Lamarque, J.-F., Lee, D., Mendoza, B., Nakajima, T., Robock, A., Stephens, G., Takemura, T., and Zhang, H.: Anthropogenic and natural radiative forcing, in: Climate Change 2013: The Physical Science Basis. Contribution of Working Group I to the Fifth Assessment Report of the Intergovernmental Panel on Climate Change, edited by: Stocker, T., Qin, D., Plattner, G.-K., Tignor, M., Allen, S., Boschung, J., Nauels, A., Xia, Y., Bex, V., and Midgley, P., 659–740, Cambridge University Press, Cambridge, United Kingdom and New York, NY, USA, doi:10.1017/CBO9781107415324.018, 2013.

Naggar, S. E. D. E.: The expedition of the research vessel "Polarstern" to the Antarctic in 2011 (ANT-XXVIII/1), available

at: http://hdl.handle.net/10013/epic.40417 (last access: 18 January 2017), 2012.

Oetjen, H., Wittrock, F., Richter, A., Chipperfield, M. P., Medeke, T., Sheode, N., Sinnhuber, B.-M., Sinnhuber, M., and Burrows, J. P.: Evaluation of stratospheric chlorine chemistry for the Arctic spring 2005 using modelled and measured OClO column densities, Atmos. Chem. Phys., 11, 689–703, doi:10.5194/acp-11-689-2011, 2011.

Ortega, I., Berg, L. K., Ferrare, R. A., Hair, J. W., Hostetler, C. A., and Volkamer, R.: Elevated aerosol layers modify the O2-O2 absorption measured by ground-based MAX-DOAS, J. Quant. Spectrosc. Ra., 176, 34–49, doi:10.1016/j.jqsrt.2016.02.021, 2016.

Partridge, H. and Schwenke, D. W.: The determination of an accurate isotope dependent potential energy surface for water from extensive ab initio calculations and experimental data, J. Chem. Phys., 106, 4618–4639, 1997.

Perner, D. and Platt, U.: Detection of Nitrous Acid in the Atmosphere by Differential OpticalAbsorption, Geophys. Res. Lett., 6, 917–920, 1979.

Peters, E., Wittrock, F., Richter, A., Alvarado, L. M. A., Rozanov, V. V., and Burrows, J. P.: Liquid water absorption and scattering effects in DOAS retrievals over oceans, Atmos. Meas. Tech., 7, 4203–4221, doi:10.5194/amt-7-4203-2014, 2014.

Pfeilsticker, K., Bösch, H., Camy-Peyret, C., Fitzenberger, R., Harder, H., and Osterkamp, H.: First atmospheric profile measurements of UV/visible O4 absorption band intensities: Implications for the spectroscopy, and the formation enthalpy of the O2-O2 dimer, Geophys. Res. Lett., 28, 4595–4598, doi:10.1029/2001GL013734, 2001.

Pinardi, G., Van Roozendael, M., Abuhassan, N., Adams, C., Cede, A., Clémer, K., Fayt, C., Frieß, U., Gil, M., Herman, J., Hermans, C., Hendrick, F., Irie, H., Merlaud, A., Navarro Comas, M., Peters, E., Piters, A. J. M., Puentedura, O., Richter, A., Schönhardt, A., Shaiganfar, R., Spinei, E., Strong, K., Takashima, H., Vrekoussis, M., Wagner, T., Wittrock, F., and Yilmaz, S.: MAX-DOAS formaldehyde slant column measurements during CINDI: intercomparison and analysis improvement, Atmos. Meas. Tech., 6, 167–185, doi:10.5194/amt-6-167-2013, 2013.

Platt, U. and Stutz, J.: Differential optical absorption spectroscopy, Springer, Berlin, Heidelberg, ISBN-13: 978-3-540-21193-8 (Print), ISBN-13: 978-3-540-75776-4 (Online), 2008.

Platt, U., Marquard, L., Wagner, T., and Perner, D.: Corrections for Zenith Scattered Light DOAS, Geophys. Res. Lett., 24, 1759–1762, 1997.

Pöhler, D., Vogel, L., Frieß U., and Platt, U.: Observation of halogen species in the Amundsen Gulf, Arctic, by active long-path differential optical absorption spectroscopy, P. Natl. Acad. Sci. USA, 107, 6582–6587, doi:10.1073/pnas.0912231107, 2010.

Polyansky, O. L., Kyuberis, A. A., Zobov, N. F., Tennyson, J., Yurchenko, S. N., and Lodi, L.: ExoMol molecular line lists XXI: Calculation of complete water linelist up to dissociation, Mon. Not. R. Astron. Soc., in preparation, 2017.

Pukīte, J., Kühl, S., Deutschmann, T., Platt, U., and Wagner, T.: Extending differential optical absorption spectroscopy for limb measurements in the UV, Atmos. Meas. Tech., 3, 631–653, doi:10.5194/amt-3-631-2010, 2010.

Regalia, L., Oudot, C., Mikhailenko, S., Wang, L., Thomas, X., Jenouvrier, A., and Von der Heyden, P.: Water vapor line param-

eters from 6450 to 9400 cm^{-1}, J. Quant. Spectrosc. Ra., 136, 119–136, 2014.

Richter, A., Wittrock, F., Ladstätter-Weißenmayer, A., and Burrows, J.: GOME measurements of stratospheric and tropospheric BrO, Adv. Space Res., 29, 1667–1672, doi:10.1016/S0273-1177(02)00123-0, 2002.

Rothman, L., Gordon, I., Barbe, A., Benner, D., Bernath, P., Birk, M., Boudon, V., Brown, L., Campargue, A., Champion, J.-P., Chance, K., Coudert, L., Dana, V., Devi, V., Fally, S., Flaud, J.-M., Gamache, R., Goldman, A., Jacquemart, D., Kleiner, I., Lacome, N., Lafferty, W., Mandin, J.-Y., Massie, S., Mikhailenko, S., Miller, C., Moazzen-Ahmadi, N., Naumenko, O., Nikitin, A., Orphal, J., Perevalov, V., Perrin, A., Predoi-Cross, A., Rinsland, C., Rotger, M., Šimečková, M., Smith, M., Sung, K., Tashkun, S., Tennyson, J., Toth, R., Vandaele, A., and Auwera, J. V.: The HITRAN 2008 molecular spectroscopic database, J. Quant. Spectrosc. Ra., 110, 533–572, doi:10.1016/j.jqsrt.2009.02.013, 2009.

Rothman, L., Gordon, I., Barber, R., Dothe, H., Gamache, R., Goldman, A., Perevalov, V., Tashkun, S., and Tennyson, J.: HITEMP, the high-temperature molecular spectroscopic database, J. Quant. Spectrosc. Ra., 111, 2139–2150, doi:10.1016/j.jqsrt.2010.05.001, xVIth Symposium on High Resolution Molecular Spectroscopy (HighRus-2009), 2010.

Rothman, L., Gordon, I., Babikov, Y., Barbe, A., Benner, D. C., Bernath, P., Birk, M., Bizzocchi, L., Boudon, V., Brown, L., Campargue, A., Chance, K., Cohen, E., Coudert, L., Devi, V., Drouin, B., Fayt, A., Flaud, J.-M., Gamache, R., Harrison, J., Hartmann, J.-M., Hill, C., Hodges, J., Jacquemart, D., Jolly, A., Lamouroux, J., Roy, R. L., Li, G., Long, D., Lyulin, O., Mackie, C., Massie, S., Mikhailenko, S., Müller, H., Naumenko, O., Nikitin, A., Orphal, J., Perevalov, V., Perrin, A., Polovtseva, E., Richard, C., Smith, M., Starikova, E., Sung, K., Tashkun, S., Tennyson, J., Toon, G., Tyuterev, V., and Wagner, G.: The HITRAN2012 molecular spectroscopic database, J. Quant. Spectrosc. Ra., 130, 4–50, doi:10.1016/j.jqsrt.2013.07.002, hITRAN2012 special issue, 2013.

Saiz-Lopez, A. and von Glasow, R.: Reactive halogen chemistry in the troposphere, Chem. Soc. Rev., 41, 6448–6472, doi:10.1039/C2CS35208G, 2012.

Sansonetti, C. J., Salit, M. L., and Reader, J.: Wavelengths of spectral lines in mercury pencil lamps, Appl. Opt., 35, 74–77, doi:10.1364/AO.35.000074, 1996.

Schwenke, D. W. and Partridge, H.: Convergence testing of the analytic representation of an ab initio dipole moment function for water: improved fitting yields improved intensities, J. Chem. Phys., 113, 6592–6597, 2000.

Serdyuchenko, A., Gorshelev, V., Weber, M., Chehade, W., and Burrows, J. P.: High spectral resolution ozone absorption cross-sections – Part 2: Temperature dependence, Atmos. Meas. Tech., 7, 625–636, doi:10.5194/amt-7-625-2014, 2014.

Shefov, N. N.: Intensivnosti nokotorykh emissiy sumerochnogo i nochnogo neba (Intensities of some Emissions of the Twilight and Night Sky), Spectral, electrophotometrical and radar researches of aurorae and airglow, IGY program, section IV, 1, 25, 1959.

Smirnov, A., Holben, B. N., Slutsker, I., Giles, D. M., McClain, C. R., Eck, T. F., Sakerin, S. M., Macke, A., Croot, P., Zibordi, G., Quinn, P. K., Sciare, J., Kinne, S., Harvey, M., Smyth, T. J., Piketh, S., Zielinski, T., Proshutinsky, A.,

Goes, J. I., Nelson, N. B., Larouche, P., Radionov, V. F., Goloub, P., Krishna Moorthy, K., Matarrese, R., Robertson, E. J., and Jourdin, F.: Maritime Aerosol Network as a component of Aerosol Robotic Network, J. Geophys. Res.-Atmos., 114, D06204, doi:10.1029/2008JD011257, 2009.

Solomon, S., Mount, H. G., Sanders, R. W., and Schmeltekopf, A. L.: Visible spectroscopy at McMurdo station, Antarctica 2. Observations of OClO, J. Geophys. Res., 92, 8329–8338, 1987.

Spinei, E., Cede, A., Herman, J., Mount, G. H., Eloranta, E., Morley, B., Baidar, S., Dix, B., Ortega, I., Koenig, T., and Volkamer, R.: Ground-based direct-sun DOAS and airborne MAX-DOAS measurements of the collision-induced oxygen complex, O_2O_2, absorption with significant pressure and temperature differences, Atmos. Meas. Tech., 8, 793–809, doi:10.5194/amt-8-793-2015, 2015.

Stutz, J. and Platt, U.: Numerical Analysis and Estimation of the Statistical Error of Differential Optical Absorption Spectroscopy Measurements with Least-Squares methods, Appl. Opt., 35, 6041–6053, 1996.

Stutz, J., Kim, E. S., Platt, U., Bruno, P., Perrino, C., and Febo, A.: UV-visible Absorption Cross-Section of Nitrous Acid, J. Geophys. Res., 105, 14585–14592, 1999.

Tennyson, J.: Vibration–rotation transition dipoles from first principles, J. Mol. Spectrosc., 298, 1–6, 2014.

Tennyson, J. and Yurchenko, S. N.: ExoMol: molecular line lists for exoplanet and other atmospheres, Mon. Not. R. Astron. Soc., 425, 21–33, 2012.

Tennyson, J., Kostin, M. A., Barletta, P., Harris, G. J., Polyansky, O. L., Ramanlal, J., and Zobov, N. F.: DVR3D: a program suite for the calculation of rotation-vibration spectra of triatomic molecules, Comput. Phys. Commun., 163, 85–116, 2004.

Tennyson, J., Bernath, P. F., Brown, L. R., Campargue, A., Carleer, M. R., Császár, A. G., Daumont, L., Gamache, R. R., Hodges, J. T., Naumenko, O. V., Polyansky, O. L., Rothmam, L. S., Vandaele, A. C., Zobov, N. F., Al Derzi, A. R., Fábri, C., Fazliev, A. Z., rtenbacher, T. F., Gordon, I. E., Lodi, L., and Mizus, I. I.: IUPAC critical evaluation of the rotational-vibrational spectra of water vapor. Part III. Energy levels and transition wavenumbers for $H_2{}^{16}O$, J. Quant. Spectrosc. Ra., 117, 29–80, 2013.

Thalman, R. and Volkamer, R.: Temperature dependent absorption cross-sections of O_2–O_2 collision pairs between 340 and 630 nm and at atmospherically relevant pressure, Phys. Chem. Chem. Phys., 15, 15371–15381, doi:10.1039/C3CP50968K, 2013.

Theys, N., De Smedt, I., Van Roozendael, M., Froidevaux, L., Clarisse, L., and Hendrick, F.: First satellite detection of volcanic OClO after the eruption of Puyehue-Cordon Caulle, Geophys. Res. Lett., 41, 667–672, doi:10.1002/2013GL058416, 2014.

Vandaele, A., Hermans, C., Simon, P., Carleer, M., Colin, R., Fally, S., Merienne, M., Jenouvrier, A., and Coquart, B.: Measurements of the NO_2 absorption cross-section from 42 000 cm^{-1} to 10 000 cm^{-1} (238–1000 nm) at 220 K and 294 K, J. Quant. Spectrosc. Ra., 59, 171–184, doi:10.1016/S0022-4073(97)00168-4, atmospheric Spectroscopy Applications 96, 1998.

Vandaele, A. C., Hermans, C., and Fally, S.: Fourier transform measurements of SO_2 absorption cross sections: II.: Temperature dependence in the 29 000–44 000 cm^{-1} (227–345 nm) region, J. Quant. Spectrosc. Ra., 110, 2115–2126, 2009.

Vogel, L., Sihler, H., Lampel, J., Wagner, T., and Platt, U.: Retrieval interval mapping: a tool to visualize the impact of the spectral

retrieval range on differential optical absorption spectroscopy evaluations, Atmos. Meas. Tech., 6, 275–299, doi:10.5194/amt-6-275-2013, 2013.

Voigt, S., Orphal, J., Bogumil, K., and Burrows, J. P.: The temperature dependence (203–293 K) of the absorption cross sections of O_3 in the 230–850 nm region measured by Fourier-transform spectroscopy, J. Photoch. Photobio. A, 143, 1–9, 2001.

Volkamer, R., Baidar, S., Campos, T. L., Coburn, S., DiGangi, J. P., Dix, B., Eloranta, E. W., Koenig, T. K., Morley, B., Ortega, I., Pierce, B. R., Reeves, M., Sinreich, R., Wang, S., Zondlo, M. A., and Romashkin, P. A.: Aircraft measurements of BrO, IO, glyoxal, NO_2, H_2O, O_2–O_2 and aerosol extinction profiles in the tropics: comparison with aircraft-/ship-based in situ and lidar measurements, Atmos. Meas. Tech., 8, 2121–2148, doi:10.5194/amt-8-2121-2015, 2015.

Wagner, T., von Friedeburg, C., Wenig, M., Otten, C., and Platt, U.: UV-visible observations of atmospheric O_4 absorptions using direct moonlight and zenith-scattered sunlight for clear-sky and cloudy sky conditions, J. Geophys. Res.-Atmos., 107, AAC 3–1–AAC 3–15, doi:10.1029/2001JD001026, 4424, 2002.

Wagner, T., Heland, J., Zöger, M., and Platt, U.: A fast H_2O total column density product from GOME – Validation with in-situ aircraft measurements, Atmos. Chem. Phys., 3, 651–663, doi:10.5194/acp-3-651-2003, 2003.

Wagner, T., Dix, B., v. Friedeburg, C., Frieß, U., Sanghavi, S., Sinreich, R., and Platt, U.: MAX-DOAS O_4 measurements: A new technique to derive information on atmospheric aerosols – Principles and information content, J. Geophys. Res., 109, D22205, doi:10.1029/2004JD004904, 2004.

Wagner, T., Deutschmann, T., and Platt, U.: Determination of aerosol properties from MAX-DOAS observations of the Ring effect, Atmos. Meas. Tech., 2, 495–512, doi:10.5194/amt-2-495-2009, 2009.

Wagner, T., Andreae, M. O., Beirle, S., Dörner, S., Mies, K., and Shaiganfar, R.: MAX-DOAS observations of the total atmospheric water vapour column and comparison with independent observations, Atmos. Meas. Tech., 6, 131–149, doi:10.5194/amt-6-131-2013, 2013.

Wang, Y., Beirle, S., Hilboll, A., Jin, J., Kyuberis, A. A., Lampel, J., Li, A., Luo, Y., Lodi, L., Ma, J., Navarro, M., Ortega, I., Peters, E., Polyansky, O. L., Remmers, J., Richter, A., Rodriguez, O. P., Roozendael, M. V., Seyler, A., Tennyson, J., Volkamer, R., Xie, P., Zobov, N. F., and Wagner, T.: MAX-DOAS measurements of HONO slant column densities during the MAD-CAT campaign: inter-comparison and sensitivity studies on spectral analysis settings, Atmos. Meas. Tech. Discuss., submitted, 2016.

Wenig, M., Jähne, B., and Platt, U.: Operator representation as a new differential optical absorption spectroscopy formalism, Appl. Opt., 44, 3246–3253, doi:10.1364/AO.44.003246, 2005.

Wilson, E. M., Wenger, J. C., and Venables, D. S.: Upper limits for absorption by water vapor in the near-UV, J. Quant. Spectrosc. Ra., 170, 194–199, doi:10.1016/j.jqsrt.2015.11.015, 2016.

Wong, K. W., Tsai, C., Lefer, B., Haman, C., Grossberg, N., Brune, W. H., Ren, X., Luke, W., and Stutz, J.: Daytime HONO vertical gradients during SHARP 2009 in Houston, TX, Atmos. Chem. Phys., 12, 635–652, doi:10.5194/acp-12-635-2012, 2012.